

# The Cepheid Distance to NGC 1637: A Direct Test of the EPM Distance to SN 1999em

Douglas C. Leonard<sup>1</sup>, Shashi M. Kanbur<sup>2</sup>, Choong C. Ngeow<sup>2</sup>, and Nial R. Tanvir<sup>3</sup>

## ABSTRACT

Type II-plateau supernovae (SNe II-P) are the classic variety of core-collapse events that result from isolated, massive stars with thick hydrogen envelopes intact at the time of explosion. Their distances are now routinely estimated through two techniques: the expanding photosphere method (EPM), a primary distance-determining method, and the recently developed standard-candle method (SCM), a promising secondary technique. Using Cycle 10 *Hubble Space Telescope* (*HST*) observations, we identify 41 Cepheid variable stars in NGC 1637, the host galaxy of the most thoroughly studied SN II-P to date, SN 1999em. Remarkably, the Cepheid distance that we derive to NGC 1637,  $D = 11.7 \pm 1.0$  Mpc, is nearly 50% larger than earlier EPM distance estimates to SN 1999em. This is the first direct comparison between these two primary distance determining methods for a galaxy hosting a well-observed, spectroscopically and photometrically normal, SN II-P. Extensive consistency checks show strong evidence to support the Cepheid distance scale, so we are led to believe that either SN 1999em is in some heretofore unsuspected way an unusual SN II-P, or that the SN II-P distance scale must be revised. Assuming the latter, this one calibration yields  $H_0(\text{EPM}) = 57 \pm 15$  km s<sup>-1</sup> Mpc<sup>-1</sup> and  $H_0(\text{SCM}) = 59 \pm 11$  km s<sup>-1</sup> Mpc<sup>-1</sup>; additional calibrating galaxies are clearly desirable in order to test the robustness of both determinations of  $H_0$ .

The *HST* observations of NGC 1637 also captured the fading SN 1999em two years after explosion, providing the latest photometry ever obtained for an SN II-P. The nebular-phase photometric behavior of SN 1999em closely follows that observed for SN 1987A at similar epochs. The *V* and *I* light curves are both

---

<sup>1</sup>Five College Astronomy Department, University of Massachusetts, Amherst, MA 01003-9305; leonard@nova.astro.umass.edu

<sup>2</sup>Department of Astronomy, University of Massachusetts, Amherst, MA 01003-9305; shashi@astro.umass.edu, ngeow@nova.astro.umass.edu

<sup>3</sup>Department of Physical Science, University of Hertfordshire, College Lane, Hatfield, AL10 9AB, UK; nrt@herts.star.ac.uk

declining at rates significantly greater than the decay slope of  $^{56}\text{Co}$  predicts. This is likely due to an increasing transparency of the envelope to gamma rays, and perhaps also to the formation of dust in the cooling atmosphere of the supernova. The absolute  $V$ -band brightness of SN 1999em is  $\sim 0.25$  mag brighter than SN 1987A at the same epochs, which suggests that a slightly greater amount of radioactive  $^{56}\text{Ni}$ ,  $\sim 0.09 M_{\odot}$ , was ejected by SN 1999em than was derived for SN 1987A ( $0.075 M_{\odot}$ ).

*Subject headings:* Cepheids — distance scale — galaxies: distances and redshifts — galaxies: individual (NGC 1637) — supernovae: individual (SN 1999em)

## 1. INTRODUCTION

Direct comparisons between distances estimated by two *primary* extragalactic distance indicators are rare. The empirical period-luminosity (PL) relation of Cepheid variable stars remains the most widely used and well studied primary extragalactic distance-determining method. It currently provides our best distance estimates to over thirty nearby ( $D \lesssim 23$  Mpc) galaxies, which enable the calibration of a host of secondary distance indicators that then establish galaxy distances well into the Hubble flow. Using such measurements, three groups have independently estimated Hubble’s constant with total (statistical + systematic) reported uncertainties<sup>4</sup> of only  $\sim 10\%$ :  $H_0 = 58 \pm 6 \text{ km s}^{-1} \text{ Mpc}^{-1}$  (Tammann & Reindl 2002b, hereafter T02),  $H_0 = 67 \pm 7 \text{ km s}^{-1} \text{ Mpc}^{-1}$  (Tanvir, Ferguson, & Shanks 1999), and  $H_0 = 72 \pm 8 \text{ km s}^{-1} \text{ Mpc}^{-1}$  (Freedman et al. 2001, hereafter F01). The differences among the Hubble constants derived by the groups are a cause of concern, and may belie unaccounted systematic uncertainties arising from the calibration of the secondary distance indicators (see F01, T02, Tammann et al. 2002, and Gibson et al. 2000 for further details about the controversy).

The Cepheid-based distance scale has recently passed a stringent external test of its accuracy: for NGC 4258, the  $H_0$  Key Project (hereafter KP) distance of  $7.8 \pm 0.3 \pm 0.5$  Mpc (Newman et al. 2001) agrees well with the geometric distance determined from observations of line-emitting water masers orbiting a supermassive black hole at the galaxy’s center, of  $7.2 \pm 0.5$  Mpc (Herrnstein et al. 1999). Since the maser distance to NGC 4258 is believed

---

<sup>4</sup>In this paper we abide by the following error bar conventions: a single, unqualified error bar (i.e., not specifically labeled as “statistical” or “systematic”) represents the total (statistical and systematic, added in quadrature) uncertainty of the measurement; if two uncertainties are given, the first represents the statistical, and the second the systematic, error of the measurement.

to have few potential sources of unaccounted systematic error, it provides a robust external check on the accuracy of the Cepheid distance scale. The agreement between the Cepheid and maser distances to NGC 4258 builds confidence in the Cepheid PL relation as an accurate primary extragalactic distance indicator.

The extraordinary brightness of supernovae (SNe) has long made them attractive targets for extragalactic distance measurements as well. SNe are grouped into two main categories, based on whether the supernova (SN) results from the thermonuclear explosion of a white dwarf (Type Ia) or the core collapse and subsequent envelope ejection of a massive (initial mass  $\gtrsim 8 - 10 M_{\odot}$ ; see Woosley & Weaver 1986, and references therein) star (Types Ib, Ic, and II; see Filippenko 1997 for a general review of SN types). Recently, the standard-candle assumption for SNe Ia, coupled with empirical relations to correct “non-standard” events (Riess, Press, & Kirshner 1996; Phillips 1993), has emerged as the leading secondary distance-determination method. SNe Ia provide precise relative distances for dozens of SNe Ia at  $z \gtrsim 0.3$ , which have revealed evidence for a nonzero cosmological constant (Riess et al. 1998; Perlmutter et al. 1999).

Unlike SNe Ia, SNe II have not traditionally served as secondary distance indicators through a standard-candle assumption. Rather, through calibration with the expanding photosphere method (EPM; Kirshner & Kwan 1974), a variant of the Baade (1926) method used to determine the distance to variable stars, they have served as *primary* distance indicators, providing direct distance measurements completely independent of the Cepheid scale. “Normal” core-collapse SNe are thought to result from isolated, massive stars with thick hydrogen envelopes intact at the time of the explosion. Their light curves show a distinct  $V$ -band plateau (hence the subclassification, “SN II-P”), resulting from an enduring period ( $\sim 100$  days) of nearly constant luminosity as the hydrogen recombination wave recedes through the envelope and slowly releases the energy deposited by the shock and by radioactive decay. EPM in its most general form (see § 2.2) is *only* securely applied to SNe II-P, and not to “peculiar” core-collapse events such as those of Type II-L (“L” for their linearly declining optical light curves, lacking a  $V$ -band plateau; these events are believed to result from progenitors that have lost a substantial fraction of their hydrogen envelope prior to exploding) or those resembling SN 1987A, which showed spectral and photometric peculiarities thought to be due to the compact nature of its progenitor star (Woosley et al. 1987). From a consistently applied EPM analysis of nine normal SNe II-P spanning distances out to  $\sim 200$  Mpc, a value of  $H_0(\text{EPM}) = 71 \pm 9$  (statistical)  $\text{km s}^{-1} \text{Mpc}^{-1}$  has recently been derived (Hamuy 2001; Hubble constant obtained by averaging the six values for  $H_0$  derived by using the  $BV$ ,  $BVI$ , and  $VI$  passbands to estimate photospheric color-temperature and two different techniques to estimate photospheric velocity for each filter combination; see § 2.2).

While the statistical uncertainty in Hubble’s constant derived from EPM distances is straightforward to derive from the scatter of the EPM distances in the Hubble diagram, the external accuracy of the technique is rather hotly debated. Fueling the debate is the fact that there have never been any measurements of Cepheid variables in a galaxy that has hosted a well-observed, spectroscopically and photometrically normal, SN II-P. To be sure, Cepheid distances do exist to four galaxies that have hosted non-plateau Type II events, as well as to one poorly observed SN II-P.<sup>5</sup> However, the non-standard nature of these SNe, or their poorly estimated distances, prevent strong conclusions from being drawn (Leonard et al. 2002a).

SN 1999em, a bright, extremely well-observed SN II-P in the nearby SBc galaxy NGC 1637, presents an outstanding opportunity to finally directly test the consistency between these two primary distance techniques. It is by far the best studied normal SN II-P to date, with three independent and mutually consistent EPM distances now reported:  $7.50 \pm 0.50$  (statistical) Mpc (Hamuy et al. 2001),  $8.24 \pm 0.56$  (statistical) Mpc (Leonard et al. 2002a), and  $7.83 \pm 0.30$  (statistical) Mpc (Elmhamdi et al. 2003). (A subsequent reanalysis of the Hamuy et al. 2001 data is given by Hamuy 2001, in which 32 different EPM distances to SN 1999em are compared using slightly different implementations of the technique; a single “best” result, however, is not given.) In this paper, we present the analysis of multi-epoch Wide Field Planetary Camera 2 (WFPC2) Cycle 10 *Hubble Space Telescope* (*HST*) observations of NGC 1637, which were taken in order to derive its distance through the analysis of its Cepheid variable stars. As a bonus, photometry of SN 1999em itself is obtained from these images, permitting a study of the photometric behavior of an SN II-P two years after explosion. This is the latest photometry ever obtained for this important class of core-collapse SN.

The paper is organized as follows. We review the Cepheid PL relation and the EPM technique in § 2, and present the *HST* observations of NGC 1637 along with a description of the data reduction and photometric analysis in § 3. We identify the Cepheid variables, derive the Cepheid distance to NGC 1637, and provide a brief analysis of the late-time photometric behavior of SN 1999em in § 4. We compare the EPM and Cepheid distances to NGC 1637, and use the Cepheid calibration to derive Hubble’s constant from both the EPM and the

---

<sup>5</sup>The four non-SNe II-P are SN 1970G in NGC 5457 and SN 1979C in NGC 4321 (both Type II-L; Schmidt, Kirshner, & Eastman 1992), SN 1987A in the Large Magellanic Cloud (LMC), and SN 1989L (classified as a Type IIn by Schlegel 1990, a Type II-L by Patat et al. 1993, 1994, and a Type II-P with spectroscopic peculiarities by Schmidt et al. 1994). A Cepheid distance exists to NGC 3627, the host of the Type II-P SN 1973R. Unfortunately, SN 1973R was not well observed, and the EPM distance has a statistical uncertainty of nearly 50% (Eastman, Schmidt, & Kirshner 1996, hereafter E96).

“standard-candle method” (SCM) recently developed by Hamuy & Pinto (2002) for SNe II-P, in § 5. We summarize our conclusions in § 6. Throughout the paper, frequent reference is made to the work of the two main groups that have previously studied the Cepheid distance scale using *HST*: The KP, led by W. Freedman, and the Type Ia SNe *HST* Calibration Program, led by A. Saha, G. Tammann, and A. Sandage (hereafter STS). The most recent summary papers from each group, F01 and T02 (for KP and STS, respectively), are cited often.

## 2. Deriving Distances to Cepheids and Type II-Plateau Supernovae

Before presenting the Cepheid study of NGC 1637, we first briefly review the techniques used to measure distances to Cepheid variables through the PL relation and SNe II-P through the EPM, focusing particular attention on potential sources of *systematic* uncertainty in both techniques.

### 2.1. Cepheid Variables and the Period-Luminosity Relation

In principle, once a Cepheid variable star in a target galaxy has been identified and had its period determined and mean magnitudes measured in at least two photometric bands, estimating the distance to its host galaxy is straightforward. The fundamental equation underlying the technique is the empirical PL relation

$$M_C = a_C \log(P) + b_C, \quad (1)$$

where  $M_C$  is the intensity mean absolute magnitude of a Cepheid in photometric band  $C$ ,  $P$  its period (usually measured in days), and  $a_C$  and  $b_C$  the slope and zero-point, respectively, of the relation. The physics behind the correlation is well understood as a consequence of the period–mean density relation obeyed by pulsating stars in the region of the Hertzsprung-Russell diagram, the instability strip, where variable stars are observed (Sandage 1958; Madore & Freedman 1991). Since the LMC is nearby and thought to have little depth along the line of sight and comparatively low extinction, PL relations have traditionally been established through the examination of its Cepheids, although attempts at a Galactic PL relation have recently been made (see discussion below and in § 5.1). Since our *HST* study relies exclusively on  $V$  and  $I$  photometry, we consider only these bandpasses in what follows.

Upon adopting a set of PL relations and computing  $M_V$  and  $M_I$  through equation (1), a Cepheid’s *apparent* distance moduli are derived from its observed mean magnitudes,  $m_V$

and  $m_I$ , as

$$\begin{aligned}\mu_V &\equiv m_V - M_V, \\ \mu_I &\equiv m_I - M_I.\end{aligned}\tag{2}$$

These apparent distance moduli are then duly corrected for extinction,

$$\mu_W \equiv \mu_V - A_V = \mu_I - A_I,\tag{3}$$

where  $A_V$  and  $A_I$  represent the extinction in the  $V$  and  $I$  bands, respectively, and the subscript  $W$  refers to the ‘‘Wesenheit reddening-free index’’ (Madore 1982; Tanvir 1997), which for  $VI$  photometry is defined as  $m_W \equiv m_V - R(m_V - m_I)$ ; this index is discussed in more detail later in this section. From equation (3) we see that

$$\mu_V - \mu_I = A_V - A_I,\tag{4}$$

which simply expresses the fact that, absent measurement or other systematic errors (see discussion by Saha, Labhardt, & Prosser 2000),  $\mu_V$  will exceed  $\mu_I$  by the difference between the extinction in the two passbands. Equations (2), (3), and (4) are then combined with the relation

$$R \equiv \frac{A_V}{A_V - A_I},\tag{5}$$

where  $R$  is typically taken to be 2.45 (derived from the extinction curve of Cardelli, Clayton, & Mathis 1989), to produce the unreddened distance modulus of the Cepheid:

$$\mu_W = \mu_V - R(\mu_V - \mu_I).\tag{6}$$

The unweighted mean,  $\overline{\mu_W}$ , of all of the individually determined Cepheid distance moduli (typically a few dozen for an *HST* target galaxy) then provides the distance modulus of the galaxy (uncorrected for possible metallicity effects, see discussion below). The use of a weighting scheme to combine the individual Cepheid distance moduli is avoided since quantifiable photometric errors are believed to be less significant than the effects that the width of the intrinsic PL relation and other systematics have on the individual distances.

For ease of analysis, equation (1) is often written explicitly in terms of the equivalent reddening-free index,  $W$ , such that

$$M_W \equiv a_W \log(P) + b_W,\tag{7}$$

and

$$\begin{aligned}\mu_W &\equiv m_W - M_W \\ &= m_W - (a_W \log[P] + b_W),\end{aligned}\tag{8}$$

where  $M_W = M_V - R(M_V - M_I)$ ,  $m_W = m_V - R(m_V - m_I)$ ,  $a_W = a_V - R(a_V - a_I)$ , and  $b_W = b_V - R(b_V - b_I)$ . Equation (8) is formally identical to equation (6). The advantage of the Wesenheit approach is that the “reddening corrected” PL relation (i.e.,  $\log(P)$  vs.  $m_W$ ) for a sample of Cepheids is intrinsically tighter than the PL relations in either band individually, and, at least in principle, permits analysis without the complicating effects of extinction.

Using *HST*, the preceding technique (or one closely similar to it) has been applied to Cepheid variables (generally with  $10 < P < 60$  days) in over 30 galaxies, providing distances to each galaxy with typical *statistical* uncertainties (e.g.,  $\sigma[m_W]/\sqrt{n-1}$ , where  $n$  is the number of Cepheids identified in the galaxy) of  $\lesssim 5\%$ . Despite intense effort during the past decade, however, significant *systematic* uncertainty still exists, and is important to quantify; detailed discussions are provided by Tammann et al. (2002), T02 and F01. For our Cepheid distance determination to NGC 1637, we identify the following five sources of systematic uncertainty:

1. *Zero point of the PL relation.* The LMC distance modulus currently sets the zero-point of the PL relations, and therefore has a direct effect on inferred Cepheid distances to other galaxies. By considering dozens of independent distance estimates to the LMC, F01 adopt a value of  $\mu_{\text{LMC}} = 18.50 \pm 0.1$  mag ( $50.1 \pm 2.3$  kpc). Using a similar but somewhat more selective approach, T02 derive  $\mu_{\text{LMC}} = 18.56 \pm 0.02$  mag. We conservatively adopt 0.1 mag for the zero-point uncertainty, and select  $\mu_{\text{LMC}} = 18.50$  mag as the distance modulus of the LMC.

2. *Metallicity.* Empirical and theoretical evidence suggests that the Cepheid PL relation has a small dependence on metallicity (Kennicutt et al. 1998; Sasselov et al. 1997; Kochanek 1997; Bono, Castellani, & Marconi 2000). Such a dependence necessitates the use of a “metallicity correction term”,  $\delta\mu_Z$ , which is dependent on the metallicity difference between the target galaxy and the galaxy used to derive the PL relations (e.g., the LMC), to correct the unreddened distance modulus,  $\mu_W$  (eq. [8]). This is accomplished by deriving the “true” distance modulus,  $\mu_0$ , as

$$\mu_0 = \mu_W + \delta\mu_Z. \tag{9}$$

The value of the correction term is still uncertain. Ultimately, F01 adopt<sup>6</sup>:

$$\delta\mu_Z = (0.2 \pm 0.2)([\text{O}/\text{H}]_{\text{galaxy}} - [\text{O}/\text{H}]_{\text{LMC}}), \tag{10}$$

---

<sup>6</sup>Note that the metallicity correction equation given by F01,  $\delta\mu_Z = (-0.2 \pm 0.2)([\text{O}/\text{H}]_{\text{galaxy}} - [\text{O}/\text{H}]_{\text{LMC}})$ , evidently contains a sign error, since the metallicity corrections derived by F01 for individual galaxies are consistent with equation (10) of the present paper.

where  $[O/H] \equiv 12 + \log O/H$ . The uncertainty contributed to the final distance is therefore a direct function of the metallicity difference between the target galaxy and the LMC. The metallicity of a galaxy,  $[O/H]_{\text{galaxy}}$ , is typically determined from H II region studies. For the LMC,  $[O/H]_{\text{LMC}} = 8.50$ . For NGC 1637, the mean metallicity of the 15 H II regions studied by van Zee et al. (1998) yields  $[O/H]_{\text{NGC1637}} = 9.08$ . (The van Zee et al. study is also consistent with the recent detailed study of a single H II region in NGC 1637 by Castellanos, Díaz, & Terlevich 2002.) The higher metallicity of NGC 1637 compared with the LMC implies a correction to its unreddened Cepheid distance of  $\delta\mu_Z = 0.12 \pm 0.12$  mag, which we adopt.

3. *Slope of the PL relations.* The values of  $a_V$  and  $a_I$  in equation (1) are the subjects of ongoing refinement and controversy, and represent an area of disagreement between the methodologies of the KP and STS groups. Table 1 lists four determinations of their values, and the zero points,  $b_V$  and  $b_I$ , that result from assuming  $\mu_{\text{LMC}} = 18.50$  mag for the relations derived from LMC Cepheids (note that in the latest STS paper by Thim et al. 2003, an LMC distance modulus of 18.50 mag is adopted). The Cepheid samples used to derive the four PL relations are as follows.

*Set A:* Photometry of  $\sim 650$  LMC Cepheids with periods ranging from 2.5 to 31 days that were observed as part of the Optical Gravitational Lensing Experiment (OGLE; Udalski et al. 1999). The PL relations are those of F01.

*Set B:* A sample of 32 Cepheids in the LMC with  $1.6 < P < 63$  days, presented by Madore & Freedman (1991).

*Set C:* The OGLE LMC Cepheid sample from Set A (above), but restricted to the 44 Cepheids with  $P > 10$  days. The PL relations are those of Thim et al. (2003).

*Set D:* 53 Galactic Cepheids drawn from the samples of Feast (1999) and Gieren, Fouque, & Gomez (1998). The PL relations are those of Thim et al. (2003).

In the final KP paper, F01 adopt the PL relations defined by Set A, and apply metallicity corrections as given by equations (9) and (10). In the most recent paper from the STS group, Thim et al. (2003) derive the distance to NGC 5236 by taking the *average* of the distances found by applying the relations defined by Sets B, C, and D individually, with no metallicity correction. Thorough discussions of the relative merits of different PL relations are given by Tanvir (1999) and Kanbur et al. (2003). For our present study, we shall follow the KP approach, and use the PL relations defined by Set A to determine the distance to NGC 1637. However, to help gauge the influence that the adopted PL relation makes on our derived distance, we shall also determine the distance to NGC 1637 using the STS methodology for comparison (see § 5.1).

Recent assessments of the systematic uncertainty contributed by the uncertainty in the slope of the PL relation are given by Tammann et al. (2002), who find that the slope uncertainty may contribute as much as a 6% (0.13 mag) systematic uncertainty to the Cepheid distance scale, and Sebo et al. (2002), who posit an  $\sim 0.06$  mag maximum contribution. Since much of the slope differences may in fact be caused by metallicity differences (Tammann & Reindl 2002a), for which a separate contribution has already been included, we adopt the smaller, 0.06 mag, estimate for the uncertainty; we shall show in § 5.1 that, at least for NGC 1637, this appears to be an appropriate uncertainty estimate.

4. *Aperture corrections.* All photometric measurements in our study were made using the HSTphot stellar photometry package (Dolphin 2000), and are detailed in § 3.2. Since the NGC 1637 field lacks bright, isolated stars from which to produce empirical aperture corrections, we adopt the default aperture corrections for the F555W and F814W filters, for which the HSTphot manual<sup>7</sup> assigns an uncertainty of 0.02 mag.

5. *WFPC2 zero point.* We adopt the estimate by Parodi et al. (2000) of 0.04 mag for the uncertainty in the WFPC2 zero point.

The sources of systematic uncertainty are summarized in Table 2. Adding them together in quadrature yields a total systematic uncertainty for the Cepheid technique of 0.17 mag, or somewhat less than 10%, for our Cepheid distance estimate to NGC 1637.

## 2.2. The Expanding Photosphere Method

### 2.2.1. The EPM Technique

Since a thorough review of EPM is given by Leonard et al. (2002a), we provide only a brief summary of the method here. In essence, EPM is a geometrical technique: the linear radius of the expanding SN photosphere,  $R$ , is compared with its angular size,  $\theta$ , to derive the distance to the SN,  $D$ . Naturally, since all extragalactic SNe are unresolved during the “photospheric” phase (the plateau in an SN II-P),  $R$  and  $\theta$  must be derived rather than measured directly. Briefly, the radial velocity of the expanding photosphere,  $v$ , is found from the Doppler shifting of the spectral lines Kirshner & Kwan (1974), so that  $R = v(t - t_0)$ , where  $(t - t_0)$  is the time since explosion and the SN is assumed to be in free expansion. The photosphere’s theoretical angular size,  $\theta$ , is calculated by comparing the observed flux with that predicted from theoretical models (e.g., a “dilute” blackbody; Wagoner 1982) for

---

<sup>7</sup>HSTphot user manual available at <http://www.noao.edu/staff/dolphin/hstphot/>.

a spherical SN photosphere as

$$\theta = \sqrt{\frac{f_{\nu} 10^{0.4A_{\nu}}}{\zeta_{\nu}^2(T_c) \pi B_{\nu}(T_c)}}, \quad (11)$$

where  $B$  is the Planck function at color temperature  $T_c$ ,  $f$  is the flux density received at Earth,  $A$  is the extinction, and  $\zeta(T_c)$  is the theoretically derived “dilution factor.” Because accurate spectrophotometry is generally not available, equation (11) is typically recast in terms of broadband photometry, with  $T_c$  and  $\zeta$  derived for some subset of  $BVIJHK$ . Since the spectral and photometric data are usually not coincident with each other, an interpolation of either the photometry to the epochs of the spectral observations (the preferred technique when many spectra with good temporal sampling exist) or the photospheric velocity measurements derived from the spectra to the times of the photometry (used when few spectra are available, which is more typically the case) must be made.

With  $R$  and  $\theta$  known,  $D$  can be found since  $\theta = R/D$  in the small-angle approximation. The greater the number of observational epochs (a minimum of 2 is required), the more precise  $D$  becomes; in essence, each observational epoch of the SN provides an independent estimate of its distance.

### 2.2.2. Sources of Statistical Uncertainty

By analyzing the scatter in the EPM Hubble diagram, Hamuy (2001) finds that the internal consistency among EPM distances indicates an average statistical uncertainty of  $\sim 20\%$  for an EPM distance measurement, a value that implicitly includes all of the contributions from *statistical* errors in photometry, photospheric velocity measurements, extinction, dilution factors, and peculiar motions of the host galaxies. This value also necessarily includes any effects resulting from departures from sphericity of SN II-P photospheres which would lead to a directionally dependent luminosity and, hence, derived EPM distance. This leads Hamuy (2001) to conclude that such departures must on average be small, since the other sources, which are more easily quantified, can easily account for a 20% statistical uncertainty without needing to include a contribution from asphericity. This contention is consistent with spectropolarimetric studies of core-collapse SNe, which also find weak evidence for asphericity during the plateau phase for SNe II-P (polarimetry directly probes asphericity since in general the greater the polarization, the greater the implied asphericity; see, e.g., Leonard, Filippenko, & Matheson 2000; Leonard & Filippenko 2001). In fact, the most thorough spectropolarimetric investigation of the sphericity assumption for an SN II-P is for SN 1999em itself, for which Leonard et al. (2001) report a very low intrinsic polarization which, for most viewing orientations and plausible geometries, suggests a substantially spherical electron-

scattering atmosphere (e.g., Höflich 1991). Ongoing spectropolarimetric studies of SNe II-P continue to support the contention that asphericity is not a major concern for the EPM technique.

A typical statistical uncertainty in an EPM distance measurement is therefore  $\sim 20\%$ . For an extremely well observed SN II-P like SN 1999em, quantifiable sources of statistical uncertainty may be even smaller, as suggested by the  $\sim 10\%$  uncertainties assigned by Hamuy et al. (2001), Leonard et al. (2002a), and Elmhamdi et al. (2003) for their EPM distance estimates of this event.

### 2.2.3. Sources of Systematic Uncertainty

While the internal precision of the EPM is fairly straightforward to constrain, the external accuracy of the technique is not. Unlike the case for Cepheids (§ 1), no rigorous external check of the accuracy of the EPM technique for an SN II-P has been carried out prior to the present study. It is generally agreed that the largest potential source of systematic error in applying the EPM to SNe II-P is the theoretically derived dilution factor,  $\zeta(T_c)$ , discussed in the previous section. Accurate knowledge of  $\zeta(T_c)$  is of paramount importance since it directly impacts derived distances, in some cases by over a factor of two; in fact, it is often referred to as the “distance correction factor,” since it “corrects” EPM-derived distances such that

$$D_{\text{actual}} = \zeta D_{\text{measured}}, \quad (12)$$

where  $D_{\text{measured}}$  is the distance derived without its inclusion in equation (11). In principle, the dilution factor could depend on many things, including the chemical composition (i.e., the metallicity) and density structure of the progenitor star, and the expansion rate and luminosity of the SN explosion. However, studies of theoretical models of realistic SN atmospheres with a wide range of properties have demonstrated that  $\zeta$  is in fact a nearly one-dimensional function of color temperature,  $T_c$  (E96; Montes & Wagoner 1995). In principle, this simple dependence on an observable quantity,  $T_c$ , allows average dilution factors to be derived from theoretical models that may then be broadly applied to *all* normal SNe II-P, and obviates the need to custom-craft individual models for particular events. Currently, the only published values of  $\zeta(T_c)$  for SNe II-P are those of E96, and so they have been used exclusively in EPM studies to date. It is important to point out again that the “generic” dilution factors of E96 are only applicable to SNe II-P, and not to “peculiar” core-collapse events, such as those in which the progenitor star is thought to have experienced substantial mass loss prior to exploding (e.g., SNe II-L, IIb, IIn, Ib, Ic), or SN 1987A-like events. While ambitious attempts have been made to apply the general dilution factors to such events

(e.g., Schmidt et al. 1992, 1993; Hamuy 2001), E96 stress that such peculiar objects require individual, detailed modeling (see, e.g., Eastman & Kirshner 1989 for detailed modeling of SN 1987A) to derive the appropriate dilution factors.

The flash point of controversy in the EPM is the fact that all modern EPM applications to normal SNe II-P have relied on dilution factors produced by only one modeling group, those published by E96 (the E96 dilution factors are based on the radiative transfer code EDDINGTON; Eastman & Pinto 1993). (The dilution factors of E96 have recently been slightly modified by Hamuy et al. 2001 to include the effects of terrestrial atmospheric absorption and to incorporate improvements in the broadband filter functions.) The values produced by this group, however, have been criticized by other modelers (e.g., Baron et al. 1995; Schmutz et al. 1990). Quantifying the degree of systematic uncertainty in the dilution factors (the E96 models show an internal statistical scatter of only  $\sim 10\%$ ) is difficult, however, since no other independent modeling group has thus far published average dilution factors directly applicable to SNe II-P.

Some insight into the situation may be gained by considering the two *unusual* core-collapse events (i.e., not normal SNe II-P) for which independent dilution factors from another group have been derived: SN 1987A in the LMC (Mitchell et al. 2002) and SN 1993J, a “Type IIb” event (Filippenko 1988) in M81 (Baron et al. 1995); see Baron, Hauschildt, & Branch (1994) for a description of the radiative transfer code, PHOENIX, used in both of these calculations. Since Leonard et al. (2002b) provide a thorough review, we just quote the result: the dilution factors produced by the PHOENIX calculations are  $\sim 50\% - 60\%$  greater than those of E96. Of course, since E96 stress that their dilution factors are only appropriate for SNe II-P, and not to peculiar variants of the SN II subclass, it is not clear how meaningful the comparison is.

Taken without consideration of the peculiar nature of the two SNe II for which they were derived, though, equation (12) implies that distances obtained using the PHOENIX-derived dilution factors would be  $\sim 50\% - 60\%$  greater than those that rely on the values given by E96. Indeed, application of the *generic* EPM prescription, using the E96 dilution factors, do yield distance estimates to these two events that are significantly shorter than those determined by other methods. For SN 1993J, Schmidt et al. (1993) derive  $D_{\text{EPM}} = 2.6 \pm 0.4$  Mpc, which is about 40% shorter than the Cepheid value for M81,  $3.63 \pm 0.13$  Mpc (F01). For SN 1987A, Hamuy (2001) derives distances ranging from 28 to 39 kpc depending on the filter set used to measure  $T_c$ . These LMC distances are significantly shorter than the accepted distance of  $\sim 50$  kpc (§ 2.1). While these comparisons are suggestive, an independently derived set of dilution factors specifically constructed for normal SNe II-P is clearly needed, so that a direct comparison with the results of E96 can be made. We shall return to this

contentious issue, and discuss current work that seeks to rectify the situation, in § 5.2.

A second potential source of systematic error arises from differences of opinion regarding the best way to estimate photospheric velocities from the spectra and to then interpolate them to derive values that are simultaneous with the photometry (from which the color temperature and, hence,  $\zeta$  are derived). Sparing the details (see Hamuy 2001, Hamuy et al. 2001, and Leonard et al. 2002a for extensive discussions), the bottom line is that the usage of different techniques and interpolation schemes can lead to significant distance discrepancies for an individual SN, in some cases of over 30% (Hamuy 2001). It is not at all clear at the present time which of the various techniques is the most appropriate one to apply, and, for now, it seems that different investigators will continue to use somewhat different methods. Indeed, Hamuy et al. (2001), Leonard et al. (2002a), and Elmhamdi et al. (2003) each use a different technique to estimate photospheric velocity in their EPM analyses of SN 1999em. Hamuy (2001) introduces yet another variation in the photospheric velocity determination, this time involving the interpolation scheme. Clearly, thorough theoretical and empirical investigations of the various techniques used to derive and interpolate photospheric velocities are needed to help clarify this potentially large source of systematic error.

Between the dilution factor and photospheric velocity, then, we must allow that the EPM distance scale may contain significant sources of systematic uncertainty, perhaps even as large as  $\sim 60\%$ . In light of the potentially large systematic uncertainty in the EPM technique compared with Cepheids ( $\sim 10\%$ ), it is clear that our Cepheid/EPM distance comparison for NGC 1637 will serve primarily as an external check on the EPM-based distance scale, and not the Cepheid scale.

#### 2.2.4. *The EPM Distance to SN 1999em*

Discovered within six days of the explosion and achieving a peak optical magnitude of  $m_V \approx 13.8$  mag (Leonard et al. 2002a), SN 1999em has taken its place as the most thoroughly studied SN II-P to date, and has been followed extensively at X-ray, UV, optical, IR, and radio wavelengths (see, e.g., Pooley et al. 2002; Leonard et al. 2002a; Hamuy et al. 2001; Baron et al. 2000; Elmhamdi et al. 2003; Berger, Kulkarni, & Chevalier 2002). Using independent data sets, three groups, all using the dilution factors of E96 (as modified slightly by Hamuy et al. 2001), have derived mutually consistent EPM distances to SN 1999em (§ 1). Taking the simple mean of the three values yields

$$\begin{aligned} \mu_0 &= 29.48 \pm 0.14 \text{ (statistical) mag, or} \\ D_{\text{EPM}} &= 7.86 \pm 0.50 \text{ (statistical) Mpc,} \end{aligned}$$

where the estimated statistical uncertainty approximates the statistical uncertainties reported for each of the three measurements, and also encompasses the internal  $1\sigma$  spread among the three individual measurements themselves. We adopt this as the “best” EPM distance estimate to SN 1999em. Although the estimated statistical uncertainty in the EPM distance is rather small, the ongoing controversies surrounding the theoretically derived dilution factors and the technique to estimate and interpolate photospheric velocity (§ 2.2.3) remain elusive gremlins in the EPM machinery, and caution us that the total uncertainty on the EPM distance may be very large.

### 3. OBSERVATIONS AND PHOTOMETRY

#### 3.1. *HST* Observations of NGC 1637

We obtained repeated images of a field containing nearly the entire visible region of NGC 1637 using the WFPC2 (Holtzman et al. 1995) on the *HST* over a 60 day period from 2001 September 02 to October 31 (*HST* observing program GO-9155). A composite mosaic image including all four chips of the instrument is shown in Figure 1. We took observations at 12 discrete epochs in the F555W passband and at six epochs in the F814W passband during the 60 day window. To facilitate removal of cosmic rays, each epoch in each filter consisted of two successive 1100 s exposures taken during one orbit. A journal of observations is given in Table 3.

The spacing of the observations was selected using a power-law time series in order to minimize period aliasing and maximize uniformity of phase coverage for the expected range of Cepheid periods, 10 – 60 days (e.g., Freedman et al. 1994). All observations were taken at the same telescope pointing and roll angle, which greatly facilitated the subsequent photometry and Cepheid identification. The frames were preprocessed through the standard Space Telescope Science Institute pipeline using the latest calibrations as of 2002 July 19.

#### 3.2. The *HST*phot WFPC2 Photometry Package

##### 3.2.1. *Image Processing*

The images were further processed using the suite of programs designed specifically for the reduction of WFPC2 data that are available as part of the *HST*phot (Dolphin 2000) software package (version 1.1; our implementation includes all updates through 2002 November 6). (Note that we adopt the convention of italicizing the names of specific tasks contained

within the HSTphot package in what follows; this convention also applies to the *hstphot* task that is contained within the HSTphot package.) We first masked bad pixels identified by the data quality images with the task *mask*, then removed cosmic rays with *crmask*, and finally combined each epoch’s cosmic-ray-split frames with *coadd*. Next, we ran *getsky* on each combined frame, which creates a “sky” frame in which the original counts in every pixel are replaced by a robust mean of the values contained in a bordered square centered on the pixel. Using these “sky” frames, the *hotpixels* task was then used to identify and mask hot pixels and to produce the final frames that were sent to the *hstphot* task for photometric analysis.

### 3.2.2. Object Identification

Following all of the preprocessing, photometric analysis was carried out using the *hstphot* task, a program that automatically accounts for WFPC2 point-spread function (PSF) variations (using a library PSF calculated from Tiny Tim [Krist 1995] models with an added residual calculated empirically from the data), charge-transfer effects across the chips, zero-points, and aperture corrections. When possible, *hstphot* returns magnitudes in standard Johnson-Cousins photometric bands (Johnson et al. 1966; Cousins 1981) as output. We ran *hstphot* with option flag 10, which combines turning on local sky determination and turning off empirically determined aperture corrections. Turning on local sky determination is recommended by the HSTphot manual for images with rapidly varying backgrounds, while turning off aperture corrections is necessary since the NGC 1637 field does not contain enough bright and isolated stars to determine a reliable empirical correction. By turning off empirical aperture corrections, default values for each filter are applied to the photometry, and are accurate, in general, to 0.02 mag (see § 2.1). We ran *hstphot* with a  $1\sigma$  detection threshold for both the combined and individual epochs, opting for such a low signal-to-noise (S/N) threshold in order to mitigate potential selection bias against fainter objects. With these input parameters, *hstphot* identified 74,307 objects in the NGC 1637 field.

### 3.2.3. Comparing HSTphot with other Photometry Packages

Photometry produced by HSTphot has been compared with that generated by other packages, including DoPHOT (Schechter, Mateo, & Saha 1993) and DAOPHOT/ALLFRAME (Stetson 1987, 1994), and the results show excellent agreement (Dolphin 2000; Saha et al. 2001a). This is not surprising, since most of the machinery of HSTphot, including the star-finding and PSF-fitting algorithms, are in fact modeled after these older packages. The

primary advantage of HSTphot is that it has built-in knowledge of WFPC2 instrumental characteristics and hence runs with far less user interaction and produces robust results that are easily reproducible by different users.

As a “sanity check” on our own implementation of HSTphot, as well as our technique for identifying and characterizing Cepheid variables (§ 4), we reduced and analyzed the archival *HST* WFPC2 data acquired for NGC 3351 as part of the KP’s Cepheid study of the galaxy (Graham et al. 1997, *HST* observing program GO-5397), using *exactly* the same techniques that were employed for the NGC 1637 data. One comparison of the photometry can be made with the 25 bright, nonvariable, comparison stars listed in Table 3 of Graham et al. (1997). The photometry reported by the KP was produced by DAOPHOT/ALLFRAME. In the *V* and *I* passbands, we derive mean differences of

$$\begin{aligned} \langle \Delta V \rangle &= 0.015 \pm 0.022 \text{ mag}, \\ \langle \Delta I \rangle &= 0.036 \pm 0.018 \text{ mag}, \end{aligned}$$

where  $\Delta V \equiv V_{\text{HSTphot}} - V_{\text{KP}}$ ,  $\Delta I \equiv I_{\text{HSTphot}} - I_{\text{KP}}$ , and the error is the standard uncertainty in the mean. While the agreement is encouraging, such a comparison is somewhat obfuscated by many subtle changes in the handling of CTE effects, aperture corrections, PSF fitting, zero-points, and so forth, that are incorporated in the recent version of HSTphot that were not available when the original KP measurements were made. More directly comparable are the final, metallicity-corrected Cepheid distances to NGC 3351:  $\mu_0$  (HSTphot) =  $30.13 \pm 0.07$  (statistical) mag, and  $\mu_0$  (KP) =  $30.00 \pm 0.09$  (statistical) mag (F01). The favorable comparison of these distance moduli provides some assurance that our photometry and analysis techniques, although somewhat different in detail from those employed by the KP, ultimately yield similar results.

## 4. RESULTS

### 4.1. Photometry of Comparison Stars

Following in the tradition established by the KP, we think it wise to list measurements of a sample of bright, unsaturated, non-variable stars on all four WFPC2 chips that can be easily remeasured at a later date for comparison. In Table 4, we list the positions and magnitudes of several such reference stars for each chip, along with the object number assigned to each star by *hstphot*. The reported positions are those of the final, combined, *V*-band frame; the positions of stars on the four WFPC2 chips are extremely consistent throughout the entire series of observations, with the maximum linear shift between any two epochs amounting to only  $\sim 1/2$  of a pixel. (Note that the X and Y positions reported by

*hstphot* are made so that an integer value is assigned to a star that is centered in the lower left corner of a pixel; this is the same convention as DoPHOT, but 0.5 lower in both X and Y than DAOPHOT.)

#### 4.2. The Late-Time Lightcurve of SN 1999em

A wonderful benefit of obtaining Cycle 10 *HST* observations of NGC 1637 is that it permits a study of the late-time photometric behavior of SN 1999em itself. At  $\sim 2$  years after the explosion, these are the latest photometric observations ever obtained for a normal SN II-P. During the nebular phase, an SN II-P is expected to have an optical lightcurve powered primarily by thermalized gamma rays resulting from the radioactive decay of  $^{56}\text{Co}$  into  $^{56}\text{Fe}$  (Woosley 1988;  $^{56}\text{Co}$  itself is the daughter of  $^{56}\text{Ni}$ , which has a half-life of only 6.1 days.) An analysis of earlier nebular-phase photometry and spectroscopy of SN 1999em is given by Elmhamdi et al. (2003), who demonstrate that SN 1999em is indeed fading in optical brightness at a rate consistent with the decay slope of  $^{56}\text{Co} \rightarrow ^{56}\text{Fe}$  of  $0.98 \text{ mag } (100 \text{ d})^{-1}$  during the time covered by their observations, which sample 180 to 508 days after explosion. A linear least squares fit to the photometric observations of Elmhamdi et al. yields slopes of  $\sim 0.97 \text{ mag } (100 \text{ d})^{-1}$  and  $\sim 1.07 \text{ mag } (100 \text{ d})^{-1}$  for the decline in  $V$  and  $I$ , respectively. In the spectral data, Elmhamdi et al. note an abrupt blueshift of spectral line profiles between days 465 and 510, and interpret this as resulting from the formation of dust in the SN atmosphere; an associated drop in optical brightness is also seen at this time. Similar spectroscopic and photometric behavior was observed in SN 1987A near 500 days after explosion as well, and was given a similar explanation (Danziger et al. 1989). Between days 500 and 750, SN 1987A exhibited an accelerating rate of decline of optical brightness along with an accompanying increase in brightness at infrared wavelengths. The spectroscopic and photometric behavior of SN 1987A during this later time have been attributed to the combined effects of newly formed dust, which extinguishes optical light and contributes thermal infrared radiation, and an increasingly transparent (to gamma rays) envelope (see Suntzeff et al. 1992, and references therein), which allows radioactive decay energy to escape without being thermalized. The dust is postulated to exist in many small, optically thick clumps, which produces nearly gray extinction (Lucy 1988).

Our *HST* observations provide 12  $V$  and 6  $I$  epochs sampling 679 to 738 days after the date of explosion of SN 1999em estimated by Leonard et al. (2002a). The results are listed in Table 5. A comparison between the absolute  $V$  and  $I$  magnitudes of SN 1999em and SN 1987A is shown in Figure 2, where the observed SN 1987A data of Hamuy & Suntzeff (1990) have been corrected for  $E(B-V) = 0.15 \text{ mag}$  (Arnett et al. 1989) and put on an

absolute scale by assuming  $\mu_{\text{LMC}} = 18.50$  mag (§ 2.1); the SN 1999em data have been corrected for  $E(B-V) = 0.10$  mag (Leonard et al. 2002a) and put on an absolute scale by using the distance modulus to NGC 1637 derived in § 4.5 (note that this distance is also ultimately based on the assumption that  $\mu_{\text{LMC}} = 18.50$  mag; § 2.1). Similar to SN 1987A at this phase, the decline rates in  $V$  and  $I$  significantly exceed the  $^{56}\text{Co}$  decay slope: a least-squares fit to our data yields decline slopes of  $1.62 \pm 0.05$  mag  $(100 \text{ d})^{-1}$  in  $V$ -band and  $2.28 \pm 0.11$  mag  $(100 \text{ d})^{-1}$  in  $I$ -band. As was inferred for SN 1987A, this is likely due to increased envelope transparency to gamma rays, and perhaps also to dust formation in the cooling SN atmosphere. Curiously, SN 1999em appears to be getting somewhat bluer with time during these epochs, within the errors. Such behavior is not seen in SN 1987A at these epochs, although it is seen at other times (see, e.g., Bouchet et al. 1996). The reason for this behavior is unclear, although variations in the strength of nebular emission lines may play a role.

The changes in slope of the “exponential tail”  $V$ -band light curve of SN 1999em appear to have closely followed those of SN 1987A, since it declined according to the exponential decay slope of  $^{56}\text{Co}$  up until about day 500, and then faded at an increasing rate similar to SN 1987A thereafter. This suggests a similar evolution of the fraction of radioactive decay energy deposited into the envelope (e.g., nearly 100% up through day 500, followed by increasing transparency thereafter). At the time covered by our *HST* observations, SN 1999em is  $\sim 0.25$  mag brighter than SN 1987A. Assuming similar bolometric corrections (e.g., Hamuy 2001, 2003) at this nebular phase for the two events (probably a reasonable assumption since the  $V$  band is essentially a continuum filter at this stage, as there are no strong emission lines in this spectral region), this implies that  $L_{99\text{em}}/L_{87\text{A}} \approx 1.26$ . From detailed modeling, Arnett (1996) estimates the mass of radioactive  $^{56}\text{Ni}$  ejected by SN 1987A to be  $0.075 M_{\odot}$ . Since nebular-phase luminosity scales in direct proportion to the amount of synthesized  $^{56}\text{Ni}$ , and SN 1999em and SN 1987A appear to have had similar energy-deposition rates during the exponential tail, this implies that  $\sim 0.09 M_{\odot}$  of  $^{56}\text{Ni}$  was synthesized and ejected by SN 1999em (cf. Elmhamdi et al. 2003).

### 4.3. Identification of Variable Stars

To identify potential variable stars among the 74,307 objects, we tested each object against a sequence of increasingly stringent selection criteria. The choice of selection criteria was guided by the philosophy that it is better to lose some real Cepheids from the sample than to include spurious or doubtful objects. We were therefore very conservative in the selection criteria used to produce the final Cepheid sample. The selection criteria, in the

order that they were applied, are as follows.

1. Object must be classified as a “point source” (as opposed to, e.g., an extended object or unresolved binary) by *hstphot*. This step eliminated 3,453 objects from further consideration.

2. Object must be more than a PSF radius away from the edge of the unvignetted portion of each chip. This eliminated 831 objects.

3. Object must be well fit by the PSF-fitting routine within *hstphot*, with reported values of  $\chi < 1.35$  and  $|\text{sharpness}| < 0.4$ . This eliminated 11,327 objects.

4. Object must have photometry reported for at least 9 *V* and 3 *I* epochs. This eliminated 22,739 objects.

5. Object must have a 99.9% chance of being variable based on the photometry and photometric uncertainty reported for all of the photometric epochs for the F555W filter (*V*-band). For this test, we applied the criterion of Saha & Hoessel (1990) that  $P(\chi_\nu^2) < 0.001$ , where

$$P(\chi_\nu^2) \equiv \int_{\chi_\nu^2}^{+\infty} \frac{x^{2[(\nu/2)-1]} e^{-x^2/2}}{2^{\nu/2} \Gamma(\nu/2)} dx^2, \quad (13)$$

and  $\nu$  is the number of degrees of freedom ( $\nu = n - 1$ , where  $n$  is the number of epochs with reported photometry),  $\Gamma$  is the gamma function, and

$$\chi^2 = \frac{1}{n-1} \sum_{i=1}^n \frac{(m_i - \bar{m})^2}{\sigma_i^2}, \quad (14)$$

where  $m_i$  is the magnitude of the  $i$ th exposure with associated uncertainty  $\sigma_i$ , and  $\bar{m}$  denotes the average over the  $n$  values of  $m_i$ . This criterion eliminated 32,221 objects from further consideration, leaving 3,736 candidate variable stars.

#### 4.4. Identification of Cepheid Variables

To distinguish Cepheids from other variables, we next fit (using weighted least-squares fitting, with weights based on the *hstphot* reported errors) each candidate variable with empirical template light curves based on a principal component description of the light curves of nearby Cepheids (see, e.g., Kanbur et al. 2002). The training data set consists of *V*- and *I*-band photometry of about 50 Cepheids with  $10 < P < 80$  days in the Magellanic Clouds and Milky Way. The photometry comes mainly from Moffett & Barnes (1984), Berdnikov & Turner (1995), Moffett et al. (1998), and Tanvir & Boyle (1999), and is well sampled

with small photometric errors. These light curves (both bands) were Fourier analysed to 12 terms (e.g., Ngeow et al. 2003), and the principle component analysis applied to vectors consisting of all of the Fourier coefficients from each band. The resulting principal component coefficients are found to be functions of period, and thus at any period we can use them to determine a range of typical light curves.

To find the period with the best-fitting template, we fit the  $V$  and  $I$  data points simultaneously, searching periods from 10 to 60 days. Setting the lower period bound at 10 days avoids contamination by first overtone pulsators and extrapolation of the PCA coefficients beyond the range defined by the template sample. The upper period limit of 60 days is set by the baseline of our observations. To arrive at the best-fitting template for each period, we solved for the best values of five free parameters: (1) phase offset between the first data epoch and the template light curve; (2) mean  $V$  magnitude; (3) mean  $I$  magnitude; (4) magnitude of the first PCA coefficient, constrained to fall within  $1.5 \sigma$  of the ridgeline established by the training-set Cepheids; and (5) magnitude of the second PCA coefficient, constrained to fall within  $1.5 \sigma$  of the ridgeline established by the training-set Cepheids (see also Ngeow et al. 2003 for the Fourier analogue of this technique). Upon arriving at the period with the best-fitting template for each candidate variable, we then tested and eliminated objects from the sample based on the following additional selection criteria (continuing the numbering from § 4.3):

6. Best-fitting template must have a “relative likelihood”  $> 0.3$ , where “relative likelihood” is defined as the quantity  $e^{-\chi^2/2\nu}$ , with  $\nu$  representing the number of degrees of freedom of the fit (e.g.,  $\nu = 12$  for a candidate with data for all 12  $V$  and 6  $I$  epochs, since there are six lost degrees of freedom from the fitting procedure), and

$$\chi^2 \equiv \sum_{i=1}^n \frac{(m_i - m_{\text{template}})^2}{\sigma_i^2}, \quad (15)$$

where  $m_i$  and  $\sigma_i$  are the data points and uncertainty, respectively, at each epoch  $i$ , and  $m_{\text{template}}$  is the value of the best-fitting template lightcurve corresponding to data epoch  $i$ . Objects with best-fitting templates that fail this criterion are considered to not have appropriately “Cepheid-like” light curves. This test eliminated 1415 objects.

7. Object must possess:

$$\frac{\text{Highest relative likelihood}}{\text{Median relative likelihood}} > 50, \quad (16)$$

over the tested period range of 10 – 60 days. This test was very effective at eliminating objects with period aliases, ultimately removing 2,279 objects from further consideration. However, while period aliasing may result from incomplete phase coverage of even bright,

well-measured objects, it is important to note that aliasing is also a natural consequence of low S/N measurements, for which (appropriately) large error bars produce a wide range of acceptable periods. For our WFPC2 photometry of NGC 1637, this begins to occur near  $V \approx 26$  mag, at which point the standard error of a magnitude determination becomes comparable to the RMS variation in the lightcurve of a Cepheid. Therefore, while this test undoubtedly eliminates many non-Cepheids, it also contains a selection bias against fainter, but potentially real, Cepheids. Such a selection bias has the potential to yield a final sample in which bright objects are overrepresented, especially at the shorter (and, hence, fainter) periods. Such an “incompleteness bias” at the faint end of a target galaxy’s apparent PL relations has been seen in previous *HST* Cepheid studies (see, e.g., F01; Saha et al. 2001b), and we must be watchful for its presence in our final Cepheid sample. The effect of this bias depends in a complex way on the selection criteria and level of correlated noise between the bands. Fortunately, the incompleteness bias usually reveals itself empirically, and is rather easily remedied by establishing a lower period cutoff for inclusion in the final set of Cepheids that are used to determine the distance to the target galaxy. The cutoff period is determined by finding the point at which the apparent distance moduli (eq. [2]) in both bands stabilize.

8. Object must have no significant (relative likelihood exceeding 0.3) aliases outside of the target range of  $10 < P < 60$  days. To check for potential short- or long-period aliases, we searched the remaining sample of 42 objects for period aliases over the extended range of 5 to 100 days. One object was eliminated from further consideration by this test.

Our selection process has therefore yielded 41 viable Cepheid candidates with well-determined periods in the range of  $10 < P < 60$  days. They are identified in Table 6. Finding charts are given in Figures 3 and 4, and light curves are shown in Figure 5. Complete photometry of the variables is given in Table 7.

As discussed in § 2.1, to determine the apparent  $V$  and  $I$  distance moduli,  $\mu_V$  and  $\mu_I$  (eq. [2]), as well as the unreddened distance moduli,  $\mu_W$  (eq. [6]), we adopt the PL relations of F01:

$$\begin{aligned} M_V &= -2.760 \log(P) - 1.458, \\ M_I &= -2.962 \log(P) - 1.942, \end{aligned} \tag{17}$$

which, through equation (7), yield

$$M_W = -3.255 \log(P) - 2.644. \tag{18}$$

As discussed in § 2.1, these PL relations were derived by F01 from photometry of  $\sim 650$  LMC Cepheids that were observed as part of the OGLE project (Udalski et al. 1999), which represents the largest study of LMC Cepheids. Given  $\mu_V$  and  $\mu_I$  for each Cepheid, it is also

possible to solve for the extinction through the relation

$$A_V = R(\mu_V - \mu_I), \quad (19)$$

where  $R = 2.45$  (see discussion in § 2.1). In Table 8, we list the periods, mean  $V$  and  $I$  magnitudes (determined as intensity-mean magnitudes, from direct integration of the best-fitting template light curves),  $A_V$ ,  $\mu_V$ ,  $\mu_I$ , and  $\mu_W$  for the Cepheid candidates. A color-magnitude diagram of all of the stars in the NGC 1637 field is shown in Figure 6. The Cepheids populate the instability strip, with some scatter likely due to reddening or measurement errors.

#### 4.5. The Cepheid Distance to NGC 1637

From the 41 Cepheids, we derive  $\overline{\mu_V} = 30.60 \pm 0.05$  (statistical) mag and  $\overline{\mu_I} = 30.39 \pm 0.04$  (statistical) mag, which implies an average extinction of  $\overline{A_V} = 0.49$  mag through equation (19). This then yields a reddening-corrected distance modulus of  $\overline{\mu_W} = 30.10 \pm 0.05$  (statistical) mag from equation (3).

The apparent PL relations in  $V$  and  $I$  for the 41 Cepheid variables are shown in Figure 7(a, b). Examination of these figures suggests that our Cepheid sample may be affected by the incompleteness bias discussed in § 4.4, since there is a preponderance of data points above the ridge lines at short periods in both bands. To test for incompleteness bias we examined how the derived apparent distance moduli for  $V$  and  $I$  change as a function of the lower cutoff period. The results are shown in Figure 8(a, b). The steady rise in the apparent distance moduli for cutoff periods below 23.0 days suggests that we are affected by incompleteness bias at these shorter periods. The degree of any bias becomes very small for cutoff periods larger than 23.0 days. We therefore adopt a lower period cutoff of  $P_{\text{cut}} = 23.0$  days ( $\log[P_{\text{cut}}] = 1.36$  days) for inclusion in the final sample, which leaves 18 Cepheids from which to derive the distance to NGC 1637.

The reddening-free PL relation is shown in Figure 7c. Taking the unweighted mean of the unreddened distance moduli for the 18 Cepheids with  $23 < P < 60$  days yields an unreddened distance modulus of  $\overline{\mu_W} = 30.23 \pm 0.07 \pm 0.17$  mag, where the systematic uncertainty is the value derived in § 2.1 and shown in Table 2. Our correction for incompleteness bias, which amounts to 0.13 mag ( $\sim 6\%$  in distance; see Fig. 8c) is somewhat larger than those typically derived in *HST* Cepheid studies (see, e.g., F01). We suspect that this is due to the conservative cut applied to the data by selection criterion 7 (§ 4.4), which removes objects with significant period aliases from the sample. As previously discussed, this criterion begins to select against fainter objects at the point where the error of a magnitude determination begins to be comparable to the RMS variation in the light curve of a Cepheid. One way

to mitigate this unwanted effect is to lower the threshold for acceptance defined by equation (16). However, while lowering this threshold does result in a larger number of Cepheid candidates being included in the final sample, the sample becomes compromised by dubious objects that sometimes yield very discrepant distances. Rather than resorting to subjective criteria or applying arbitrary cuts based on derived distance or color that would, almost inevitably, still permit some non-Cepheids to dilute the final sample, we feel that the conservative, but quantitative and objective, approach is best. In this effort we are aided by the rather large sample of Cepheids identified in the target galaxy, which enables a statistically sound sample of *bona fide* Cepheids to remain after the lower period cutoff is applied.

Applying the metallicity correction of  $\delta\mu_Z = 0.12 \pm 0.12$  mag derived in § 2.1 yields a final Cepheid distance to NGC 1637 of:

$$\begin{aligned}\mu_0 &= 30.34 \pm 0.07 \pm 0.17 \text{ mag, or} \\ D &= 11.71 \pm 0.36 \pm 0.92 \text{ Mpc,}\end{aligned}$$

through equation (9). It is immediately apparent that this distance is significantly discrepant with the EPM distance derived earlier (§ 2.2.4), in the sense that *the Cepheid distance to NGC 1637 is nearly 50% greater than the EPM distance to SN 1999em*.

## 5. DISCUSSION

### 5.1. Comparison of the Cepheid and EPM Distances to NGC 1637

The primary goal of this Cepheid study is to test and, ultimately, to calibrate the SN II-P distance scale. To derive our distance to NGC 1637, we have largely followed the procedures of the KP, as outlined by F01. As discussed in § 2.1, however, there is currently some debate between the KP and STS groups on the appropriate values to use for the slopes of the *V*- and *I*-band PL relations. Therefore, before concluding that a significant discrepancy exists between the Cepheid and EPM distance scales, it seems prudent to check our Cepheid distance against the distance that would have been derived had we adopted the current methodology of the STS group, as given by Thim et al. (2003) and described in § 2.1 (e.g., taking the mean of the distance moduli resulting from the PL relations derived from Cepheid Sets *B*, *C*, and *D* in Table 1). When this is done, a Cepheid distance of  $D_{STS} = 11.81$  Mpc ( $\mu_0[STS] = 30.36$  mag) results. This distance is in excellent agreement with the KP-derived value,  $D_{KP} = 11.71$  Mpc, and builds confidence in the robustness of the Cepheid/EPM discrepancy that we have found (as well as the uncertainty ascribed to the slope of the PL relations in § 2.1).

We therefore conclude that the EPM distance to SN 1999em of  $D_{\text{EPM}} = 7.86 \pm 0.50$  (statistical) Mpc (§ 2.2.4) is indeed inconsistent, at the  $3.5 \sigma$  level, with the Cepheid distance to NGC 1637 of  $D = 11.71 \pm 0.99$  Mpc. Since the total uncertainty in the Cepheid distance is estimated to be  $\lesssim 10\%$  whereas the EPM distance may suffer from as much as a 60% systematic uncertainty (§ 2.2.3), suspicion immediately falls on the EPM as having underestimated the distance to SN 1999em. This contention is supported by other considerations as well, which we now discuss.

## 5.2. Additional Distance Estimates to NGC 1637

Seven other estimates of the distance of NGC 1637 exist, six of which favor the longer Cepheid distance over the shorter EPM distance.

(1) *The Tully-Fisher relation.* Due to its nearly face-on orientation and somewhat lopsided disk (Ryder & Dopita 1993; Block et al. 1994), NGC 1637 is not an ideal Tully-Fisher (TF) target. Nonetheless, a *B*-band TF distance has been derived by Bottinelli et al. (1985):

$$\begin{aligned}\mu_0 &= 30.70 \pm 0.38 \text{ mag, or} \\ D &= 13.8 \pm 2.4 \text{ Mpc.}\end{aligned}$$

(2) *Inner ring structure.* By examining the diameter of the inner ring structure of NGC 1637, Buta & de Vaucouleurs (1983) derive a distance to NGC 1637 of

$$\begin{aligned}\mu_0 &= 30.23 \pm 0.69 \text{ mag, or} \\ D &= 11.12 \pm 3.53 \text{ Mpc.}\end{aligned}$$

(3) *The kinematic distance.* Adopting a Hubble constant of  $H_0 = 68 \text{ km s}^{-1} \text{ Mpc}^{-1}$ , and applying the parametric model for peculiar flows of Tonry et al. (2000), Hamuy (2003) derives a kinematic distance to NGC 1637 of

$$\begin{aligned}\mu_0 &= 30.15 \pm 0.49 \text{ (statistical) mag, or} \\ D &= 10.7 \pm 2.4 \text{ (statistical) Mpc.}\end{aligned}$$

(4) *The spectral-fitting expanding atmosphere method applied to SN 1999em.* The dilution factors of E96 (as modified slightly by Hamuy et al. 2001) were used in all three EPM estimates of the distance to SN 1999em. As discussed in § 2.2.3, however, a nagging source of uncertainty in the EPM technique is the possible disagreement among various modeling

groups of the magnitude of the theoretically derived dilution factors, which have a profound impact on EPM distances (e.g., eq. [12]). In the only direct comparisons that have been made to date, the radiative transfer models of Baron et al. (1994) have consistently yielded dilution factors that are significantly larger than those of E96, in some cases by as much as 60% (Mitchell et al. 2002; Baron et al. 1995). However, the fact that these dilution factors were produced for somewhat peculiar SNe II, and not normal SNe II-P, casts doubt on the significance of the offset, which will remain until a full, independent set of dilution factors appropriate for an SN II-P is produced.

Thankfully, such a project is now underway, and a distance to SN 1999em itself is currently being derived by E. Baron and collaborators using the PHOENIX radiative transfer code (Baron et al. 1994). The technique being used to determine the distance is formally known as the spectral-fitting expanding atmosphere method (SEAM; Baron et al. 1993; Baron et al. 1994; Baron et al. 1995), although it is similar in spirit to EPM. Unlike the standard implementation of the EPM for which a generic set of average dilution factors for SNe II-P are used to correct distances via equation (12), however, the SEAM establishes distances through the detailed modeling of individual spectra. The fitted models provide the entire spectral energy distribution of an SN on an absolute scale, from which synthetic absolute photometry is derived. The synthetic photometry is then compared with the observed photometry and a distance modulus for each spectral epoch in each available photometric band results. There is no explicit need for dilution factors in the technique, although they may be calculated for comparison purposes. A preliminary SEAM analysis of SN 1999em (E. Baron, private communication), based on spectral fits to only the two early time spectra analyzed in the study by Baron et al. (2000), yields:

$$\begin{aligned} \mu_0 &= 31.0 \pm 0.6 \pm 0.5 \text{ mag, or} \\ D &= 15.8 \pm 4.4 \pm 3.6 \text{ Mpc.} \end{aligned}$$

The large uncertainty in this preliminary distance will undoubtedly be reduced as additional spectra are analyzed. Nonetheless, at this stage, a significant preference for the longer, Cepheid-based, distance exists, providing some support for the contention that much of the Cepheid/EPM distance discrepancy may be explained by an underestimate of the E96 dilution factors for at least this SN II-P.

(5) *Standard-candle method for SNe II-P.* SNe II-P are *not* standard candles, since they display a range in  $V$ -band plateau brightness of more than 5 mag. However, a promising empirical technique has emerged that has the potential to achieve distance estimates of SNe II-P with a precision rivaling those currently derived to SNe Ia (e.g.,  $\sim 10\%$ ). Developed by Hamuy & Pinto (2002), the method treats SNe II-P as “calibratable standard candles” by adjusting individual luminosity differences through the use of an empirically derived

relationship between expansion velocity (as determined from the blueshift of spectral lines) and luminosity (in the sense that brighter SNe II-P have higher expansion velocities). This type of empirical correction is quite similar in spirit to the accepted  $\Delta m_{15}$  (Phillips 1993) and multicolor light-curve shape (Riess et al. 1996) methods that are used to adjust SNe Ia luminosities to a “standard” value. The initial results of the SCM for SNe II-P are impressive: from a sample of 16 SNe II-P, Hamuy & Pinto (2002) find that the correlation between expansion velocity and luminosity reduces the scatter in the Hubble diagram from  $\sim 1$  mag to  $\sim 0.4$  and  $\sim 0.3$  mag in the  $V$  and  $I$  bands, respectively. Further restricting the sample to objects that are well in the Hubble flow yields an even tighter result: for eight SNe II-P with  $cz > 3000$  km s $^{-1}$ , the Hubble diagram scatter drops to only 0.2 mag in both bands, or roughly 9% in distance. Compared with the EPM, which has an internal precision of  $\sim 20\%$  (§ 2.2.2), the SCM appears to be significantly more precise. It is also far easier to apply since it requires only a few photometric epochs, a single spectrum, and no theoretical modeling.

Since SCM is not a primary distance indicator, however, the zero-point of its Hubble diagram must be determined externally. Of course, prior to our present study, no host galaxy of a normal, well-observed SN II-P had its distance measured by a reliable primary distance indicator (i.e., Cepheid variables). Therefore, Hamuy & Pinto (2002) cautiously establish the SCM zero point by using SN 1987A in the LMC (assumed distance modulus of 18.50 mag), even though SN 1987A is an admittedly rather peculiar variant of the plateau subclass. Nonetheless, using the scale established by SN 1987A and the  $V$  and  $I$  plateau magnitudes and expansion velocities of SN 1999em given by Hamuy & Pinto (2002),<sup>8</sup> yields an SCM distance to SN 1999em of:

$$\begin{aligned}\mu_0 &= 30.49 \pm 0.40 \pm 0.57 \text{ mag, or} \\ D &= 12.53 \pm 2.31 \pm 3.29 \text{ Mpc,}\end{aligned}$$

from the  $V$ -band relation, and

$$\begin{aligned}\mu_0 &= 30.63 \pm 0.29 \pm 0.45 \text{ mag, or} \\ D &= 13.37 \pm 1.79 \pm 2.77 \text{ Mpc,}\end{aligned}$$

from the  $I$ -band relation. The quoted systematic uncertainties incorporate uncertainties in the slope of the calibrating SCM relations (see eqs. [1] and [2] of Hamuy & Pinto 2002), the extinction ( $\sigma[A_V] = 0.3$  mag;  $\sigma[A_I] = 0.18$  mag), plateau magnitude ( $\sigma[V_p] = 0.05$

---

<sup>8</sup>Note that the expansion velocity of SN 1999em given by Hamuy & Pinto (2002), of  $v = 3557$  km s $^{-1}$ , has a typographical error (M. Hamuy, personal communication). The correct value,  $v = 3757$  km s $^{-1}$ , is given by Hamuy (2003).

mag;  $\sigma[I_p] = 0.05$  mag), photospheric velocity ( $\sigma[v_p] = 300$  km s<sup>-1</sup>), and distance modulus of SN 1987A ( $\sigma[\mu_0] = 0.1$  mag). It does not include the (unknown) systematic uncertainty added by the fact that SN 1987A was not a typical SN II-P. The statistical errors result from the uncertainty in the extinction ( $\sigma[A_V] = 0.3$  mag;  $\sigma[A_I] = 0.18$  mag), plateau magnitude ( $\sigma[V_p] = 0.05$  mag;  $\sigma[I_p] = 0.05$  mag), and photospheric velocity ( $\sigma[v_p] = 300$  km s<sup>-1</sup>) of SN 1999em. The *V*- and *I*-band distances yield an average estimate of about  $13 \pm 4$  Mpc. It must be noted that since the zero points of both the SCM and the Cepheid PL relation are set by the LMC distance modulus, the ultimate calibrations of the two techniques are not completely independent, and share the same systematic uncertainty (0.1 mag) contributed by the uncertainty in the LMC distance.

(6) *Plateau-tail method for SNe II-P*. Motivated primarily by theoretical considerations, Nadyozhin (2003) has recently introduced a novel way to estimate distances to SNe II-P that involves both the plateau and exponential tail luminosities as well as the photospheric velocity during the plateau. For SN 1999em, he finds

$$\begin{aligned}\mu_0 &= 30.2 \pm 0.4 \text{ (statistical) mag, or} \\ D &= 11.1 \pm 2.2 \text{ (statistical) Mpc,}\end{aligned}$$

where the uncertainty has been estimated from the average scatter of the plateau-tail distances derived by Nadyozhin (2003) about the Hubble line for the eight SNe II-P considered in the study. These SNe II-P also have earlier EPM distance estimates, and it is interesting to note that Nadyozhin (2003) finds an average distance discrepancy between the two techniques of  $\sim 25\%$ , in the sense that  $D_{\text{EPM}}$  is systematically *shorter* than  $D_{\text{plateau-tail}}$ .

(7) *Brightest red supergiants*. Treating the brightest red supergiants (BRSG) detected in ground-based images of NGC 1637 as standard candles, Sohn & Davidge (1998) derive

$$\begin{aligned}\mu_0 &= 29.47 \pm 0.27 \text{ (statistical) mag, or} \\ D &= 7.8_{-0.9}^{+1.0} \text{ (statistical) Mpc,}\end{aligned}$$

where the stated error accounts for the difficulty of identifying the BRSG and a correction for crowding effects.

Since the BRSG technique provides the only distance estimate that favors the shorter EPM distance to NGC 1637 over the longer one determined by Cepheids, it is important to quantify its potential systematic uncertainty. The merit of the BRSG technique is that red supergiants are among the very brightest stars in a galaxy, and can be detected in a single epoch of observations. The drawbacks are that individual red supergiants can easily be confused by foreground stars, H II regions, and clusters in the target galaxy, and they are always few in number leading to weak statistical significance in most cases. Not surprisingly,

this technique has not been extensively used for distance determination in recent years. The basis for the BRSG being standard candles is primarily empirical, and according to Rozanski & Rowan-Robinson (1994) systematic uncertainties for individual galaxy distances are at least 0.5 mag in distance modulus. Adding this in quadrature to the quoted statistical error suggests that a total uncertainty of at least 0.57 mag should be adopted for the Sohn & Davidge (1998) estimate.

Of course, none of the preceding seven distance estimates to NGC 1637 are individually unassailable. Taken together, however, the fact that all but one prefer the Cepheid distance certainly provides support for the longer, Cepheid-based distance to NGC 1637. A summary of the distance measurements is given in Table 9.

### 5.3. The Progenitor Star Mystery

Smartt et al. (2002) examine pre-explosion images of NGC 1637 and use the lack of a progenitor-star detection in the pre-discovery frames, together with an assumed distance of  $D = 7.50$  Mpc from the Hamuy et al. (2001) EPM study, to determine a detection threshold for the absolute brightness of the progenitor star of SN 1999em. Smartt et al. (2002) then compare this detection threshold with the results of detailed stellar evolution calculations based on the most recent version of the Eggleton (1971, 1972, 1973) evolution program, which traces stellar luminosities through the carbon-burning phase and predicts final luminosities of core-collapse SN progenitors. From these models, Smartt et al. (2002) conclude that any progenitor star with  $M > 7 M_{\odot}$  should be detectable in the pre-explosion images. The lack of such a detection at the location of SN 1999em in these images, especially in light of the theoretical expectation that core-collapse SNe only result from progenitors with  $M \gtrsim 8 - 10 M_{\odot}$  (see Woosley & Weaver 1986, and references therein), is quite puzzling. Indeed, it is only by considering the *uncertainty* on the threshold detection limit ( $\sim 0.2$  dex), that Smartt et al. (2002) are able to (barely) explain the nondetection, and then only for a very narrow range of possible progenitor masses,  $12 \pm 1 M_{\odot}$ . However, this calculation rests squarely on the distance assumed for NGC 1637. Adopting the longer, Cepheid-based distance to NGC 1637 derived here will naturally result in a brighter intrinsic detection threshold for the progenitor star. In fact, substituting the Cepheid distance to NGC 1637 of 11.71 Mpc results in a 0.39 dex increase in the detection threshold of the pre-explosion images (see Smartt et al. 2002, Figs. 4 and 5). Adopting the 0.2 dex uncertainty on the threshold level and following exactly the same procedure as Smartt et al. (2002), we find that all progenitors with  $M < 20 M_{\odot}$  could remain undetected in the pre-explosion images. Therefore, by adopting the new Cepheid distance to NGC 1637, we derive an upper mass

limit for the progenitor of SN 1999em of  $20 \pm 5 M_{\odot}$ ; following Smartt et al. (2002), the uncertainty is simply set by the nearest modeled progenitor masses on either side of the observed limit.

The details of late-time stellar evolution are still quite controversial, and subtle changes in the evolution can lead to different conclusions. For instance, if we adopt the Geneva evolutionary tracks of Meynet et al. (1994), instead of the models of Smartt et al. (2002), a more restrictive upper limit of  $M < 15_{-3}^{+5} M_{\odot}$  results. The exact upper limit therefore remains somewhat uncertain. Nonetheless, a longer distance to NGC 1637 certainly helps to explain the absence of a progenitor star in pre-explosion images of the site of SN 1999em.

#### 5.4. Potential Causes of the EPM Distance Underestimate

The preceding discussion provides significant circumstantial evidence to favor the Cepheid distance over the EPM measurement. A most important additional consideration, of course, is that the Cepheid distance scale has already passed a stringent external check of its accuracy through its comparison with the maser distance to NGC 4258 (§ 1), whereas the EPM distance scale has not. The case for the shorter EPM distance therefore seems to us to be difficult to maintain: it agrees with only one of seven other distance estimates and leaves the puzzling non-detection of the progenitor star in potential disagreement with the results of current stellar evolution theory. Furthermore, unlike the case for the EPM, no ready explanation exists for a major alteration in the Cepheid distance scale, for which systematic uncertainties are believed to be  $\lesssim 10\%$  (§ 2.1); such an adjustment to the Cepheid scale, by inference, would also call into question the quite secure maser distance to NGC 4258. Therefore, on balance we find that the available evidence substantially favors the Cepheid distance over the EPM distance.

The obvious question, then, is why the EPM has underestimated the distance to SN 1999em. Since analysis of the scatter in the EPM Hubble diagram leads to the conclusion that the total statistical uncertainty in a typical EPM measurement is only  $\sim 20\%$  (§ 2.2.2), the likelihood of some source of statistical error being predominantly responsible for the EPM underestimate is rather remote. Of course, it is always possible that SN 1999em was in some heretofore unsuspected way an unusual SN II-P, or that several statistical sources of uncertainty have conspired to produce the result. For instance, one scenario that could plausibly explain the distance underestimate is if SN 1999em was, in fact, highly aspherical during the plateau phase. Nadyozhin (1998) demonstrates that an SN shaped as an oblate ellipsoid with an axial ratio of  $\sim 0.6$  and oriented such that the symmetry axis is directed nearly along the line-of-sight (e.g., nearly “face-on”), would yield an EPM distance that

underestimates the true distance by  $\sim 50\%$ . This particular viewing orientation would lead to very little observed polarization (e.g., Höflich 1991), and would therefore be consistent with the spectropolarimetric results of Leonard et al. (2001) as well. The difficulty with this explanation, however, is that it requires SN 1999em, by all other accounts a “normal” SN II-P, to be unique: if SNe II-P as a class are indeed as aspherical as suggested by this explanation, then random viewing orientations would yield both larger average intrinsic polarizations and significantly more scatter in the EPM-based Hubble diagram than are observed. Since there is at present no compelling indication that SN 1999em was anything but a “normal” SN II-P, we believe asphericity (or, indeed, any single statistical source of uncertainty) to be an unlikely sole agent for the EPM distance underestimate. The size of the discrepancy between the EPM and Cepheid distances to NGC 1637 therefore compels us to believe that systematic error also contributes, with the most likely sources being the dilution factor and the technique used to estimate (and interpolate) photospheric velocity (§ 2.2.3).

### 5.5. The Value of $H_0$ from SNe II-P

The Cepheid distance to SN 1999em allows the calibration of both the EPM and SCM Hubble diagrams, from which Hubble’s constant may be derived. For the EPM, the most recent estimate of  $H_0$  is that of Hamuy (2001). In this study, nine well-observed SNe II-P (including SN 1999em) are each assigned EPM distances that are derived in a consistent manner using the  $BV$ ,  $BVI$ , and  $VI$  filter combinations to estimate color-temperature and the dilution factors of E96 (as modified slightly by Hamuy et al. 2001). Photospheric velocities are estimated by two different techniques, and a power-law is fit to the velocity measurements in order to interpolate them to the epochs of the photometry (this differs from the technique followed by Hamuy et al. 2001 in which a polynomial was fit to the velocities). The use of three different filter combinations and two different sets of velocity estimates naturally results in six different distance estimates for each SN in the study and, hence, six different Hubble diagrams, from which Hamuy (2001) derives values of  $H_0$  ranging from  $67 \text{ km s}^{-1} \text{ Mpc}^{-1}$  to  $76 \text{ km s}^{-1} \text{ Mpc}^{-1}$ ; a “best” value is not given. Since at this time we have no reason to favor any particular filter set or velocity determination method, it seems reasonable to average the six values to arrive at the estimate given in § 1, of  $H_0 = 71 \pm 9$  (statistical)  $\text{km s}^{-1} \text{ Mpc}^{-1}$ .

To derive a new EPM-based value of  $H_0$ , we therefore calibrate the Hubble diagrams of Hamuy (2001) using the Cepheid distance to SN 1999em derived here, and arrive at an

average value of

$$H_0(\text{EPM}) = 57 \pm 7 \pm 13 \text{ km s}^{-1} \text{ Mpc}^{-1}$$

from the six resulting values of  $H_0$ . The statistical uncertainty in  $H_0(\text{EPM})$  is derived from the statistical scatter of the SNe II-P about the Hubble line. The systematic uncertainty incorporates the scatter of the six individual values of  $H_0$  and the uncertainty in the offsets between the Cepheid distance derived in this work and the six EPM distances to SN 1999em derived by Hamuy (2001), which includes contributions from the statistical error in the EPM distances to SN 1999em (for this we adopt the more conservative 20% uncertainty discussed in § 2.2.2) and the total uncertainty in the Cepheid distance to NGC 1637. It is important to point out that applying the NGC 1637 calibration essentially reduces EPM to the status of a secondary distance-determining method, with its ultimate calibration now provided by Cepheid variables.

For the SCM, calibrating the 16 SNe II-P in the sample analyzed by Hamuy & Pinto (2002) with the Cepheid distance to SN 1999em yields  $H_0 = 58 \pm 3 \pm 12 \text{ km s}^{-1} \text{ Mpc}^{-1}$  for the  $V$ -band relation and  $H_0 = 60 \pm 3 \pm 10 \text{ km s}^{-1} \text{ Mpc}^{-1}$  for the  $I$ -band relation. Taking the average of the two values yields

$$H_0(\text{SCM}) = 59 \pm 3 \pm 11 \text{ km s}^{-1} \text{ Mpc}^{-1}.$$

The calibrated  $V$ -band SCM Hubble diagram for this sample of SNe is shown in Figure 9. The statistical uncertainty in the Hubble constant derived from SCM is particularly impressive, and rivals that derived from SNe Ia (see, e.g., F01). The SCM therefore appears to be a promising extragalactic distance-determining method. However, true confidence in the technique requires additional, nearby SNe II-P to be calibrated by the “training set” provided by the original set of objects studied by Hamuy & Pinto (2002). Should the calibrating relations prove to be robust, the SCM could provide precise distance moduli beyond  $z \sim 0.3$ , and allow an independent check on the evidence from SNe Ia for a non-zero cosmological constant.

The estimates of  $H_0$  by both the EPM and SCM would greatly benefit from additional Cepheid calibrations. For the EPM, such calibrations will help to determine whether the Cepheid/EPM discrepancy derived here is truly universal for SNe II-P, or whether SN 1999em was in some way a (heretofore unrecognized) peculiar EPM object. For the SCM, additional calibrations could ultimately reduce the uncertainty in  $H_0$  to the  $\sim 10\%$  level currently set by the systematic uncertainty in the Cepheid distance scale. Incidentally, we note that the Hubble constants derived from the SCM calibration provided by SN 1987A,  $H_0 = 54 \pm 13 \text{ km s}^{-1} \text{ Mpc}^{-1}$  and  $H_0 = 53 \pm 10 \text{ km s}^{-1} \text{ Mpc}^{-1}$  for the  $V$  and  $I$  relations (Hamuy & Pinto 2002), respectively, are in good agreement with those derived using our Cepheid

NGC 1637 calibration. This suggests that the standard formulation of SCM may even be applicable to those SNe II that show photometric and spectroscopic peculiarity similar to SN 1987A.

The longer distance scales, and correspondingly smaller Hubble constants, established by both the EPM and SCM Hubble diagrams when calibrated with the Cepheid distance to NGC 1637 find good agreement with the conclusions of the STS group, who report  $H_0 = 58 \pm 6 \text{ km s}^{-1} \text{ Mpc}^{-1}$  (T02) from the Cepheid calibration of SNe Ia peak luminosity. The SNe II-P results are marginally inconsistent with the results of the KP, who derive  $H_0 = 72 \pm 8 \text{ km s}^{-1} \text{ Mpc}^{-1}$  (F01), from the Cepheid calibration of a variety of secondary distance indicators. Additional Cepheid calibrations to galaxies hosting SNe II-P will allow more statistically stringent comparisons to be made.

## 6. CONCLUSIONS

SN 1999em is an extremely well-studied Type II-P event, for which three independent and mutually consistent EPM distances have been derived; taking the average of the three values yields  $D_{\text{EPM}} = 7.86 \pm 0.50$  (statistical) Mpc. We present the analysis of multi-epoch WFPC2 Cycle 10 *HST* observations of NGC 1637, the host galaxy of SN 1999em, which were taken in an effort to derive its distance through the analysis of its Cepheid variable stars. This provides the first direct comparison between the EPM and Cepheid techniques for a galaxy hosting a well-observed, spectroscopically and photometrically normal, SN II-P. As a bonus, the *HST* images also contained the fading SN 1999em itself, roughly two years after it exploded, permitting an analysis of its nebular-phase photometric behavior. Our main results are as follows.

1. We identify 41 Cepheid variables in NGC 1637 with  $10 < P < 60$  days. To avoid the effects of an “incompleteness bias” that is suggested by our data at short periods, we remove the 23 Cepheids with  $P < 23$  days from the sample used to determine the final distance to NGC 1637.

2. Using the PL relations of F01, the 18 Cepheids with  $23 < P < 60$  days yield a mean distance of  $11.10 \pm 0.34 \pm 0.87$  Mpc for NGC 1637, before correcting for the effects of the metallicity difference between NGC 1637 and the LMC. Applying the metallicity correction procedure of F01 yields a final, metallicity-corrected, Cepheid distance to NGC 1637 of  $11.71 \pm 0.36 \pm 0.92$  Mpc. This distance is nearly 50% greater than the previous EPM distances to SN 1999em, and formally represents a  $3.5 \sigma$  discrepancy between the results.

3. We find compelling evidence to favor the Cepheid distance over the EPM distance,

including the fact that it (a) is in better agreement with six of seven other distance estimates to NGC 1637; (b) helps to resolve a mystery concerning the lack of a detectable progenitor star in pre-explosion images of NGC 1637; (c) is believed to suffer from much lower systematic uncertainty than the EPM distance ( $\sim 10\%$  for Cepheids compared with up to  $\sim 60\%$  for the EPM); and (d) is derived using a technique that has already passed a stringent external test of its accuracy (e.g., the maser distance to NGC 4258). We suspect that a substantial portion of the Cepheid/EPM discrepancy may be explained by an underestimate of the theoretically derived dilution factors of E96 that have been used in previous EPM distance estimates to normal SNe II-P, although other sources of statistical and systematic uncertainty may contribute as well.

4. Using the Cepheid calibration of NGC 1637, we derive Hubble’s constant for both the EPM and the promising SCM technique recently proposed by Hamuy & Pinto (2002):  $H_0(\text{EPM}) = 57 \pm 7 \pm 13 \text{ km s}^{-1} \text{ Mpc}^{-1}$  and  $H_0(\text{SCM}) = 59 \pm 3 \pm 11 \text{ km s}^{-1} \text{ Mpc}^{-1}$ . The uncertainty in both determinations of  $H_0$  can be significantly reduced by obtaining additional calibrating galaxies.

5. We analyze the photometric behavior of SN 1999em from days 679 to 738 after explosion. After correcting for the effects of reddening and distance, SN 1999em and SN 1987A are found to have similar absolute  $V$  and  $I$  magnitudes at this phase. From the comparison, we conclude that SN 1999em ejected about  $0.09 M_\odot$  of radioactive  $^{56}\text{Ni}$ , which is slightly more than was derived for SN 1987A ( $\sim 0.075 M_\odot$ ). The  $V$  and  $I$  light curves of SN 1999em and SN 1987A are also quite similar, although SN 1999em may be fading somewhat more rapidly in the  $I$  band. Both objects decline at greater rates than the decay slope of  $^{56}\text{Co}$  predicts. We postulate that increased transparency of the envelope to gamma rays, along with dust formation in the cooling atmosphere of the supernova, may explain this behavior.

This research has made use of the NASA/IPAC Extragalactic Database (NED), which is operated by the Jet Propulsion Laboratory, California Institute of Technology, under contract with NASA. We thank Dmitriy Nadyozhin, Tim Young, Mario Hamuy, and Alex Filippenko for useful discussions, and an anonymous referee for helpful suggestions that resulted in an improved manuscript. Support for program #G0-9155 was provided by NASA through a grant from the Space Telescope Science Institute, which is operated by the Association of Universities for Research in Astronomy, Inc., under NASA contract NAS 5-26555.

## REFERENCES

- Arnett, W. D. 1996, *Supernovae and Nucleosynthesis* (New Jersey: Princeton University Press)
- Arnett, W. D., Bahcall, J. N., Kirshner, R. P., & Woosley, S. E. 1989, *ARA&A*, 27, 629
- Baade, W. 1926, *Astronomische Nachrichten*, 228, 359
- Baron, E., et al. 2000, *ApJ*, 545, 444
- Baron, E., Hauschildt, P. H., & Branch, D. 1994, *ApJ*, 426, 334
- Baron, E., et al. 1995, *ApJ*, 441, 170
- Baron, E., Hauschildt, P. H., Branch, D., Wagner, R. M., Austin, S. J., Filippenko, A. V., & Matheson, T. 1993, *ApJ*, 416, L21
- Berdnikov, L. N., & Turner, D. G. 1995, *Astronomy Letters*, 21, 534
- Berger, E., Kulkarni, S. R., & Chevalier, R. A. 2002, *ApJ*, 577, L5
- Block, D. L., Bertin, G., Stockton, A., Grosbol, P., Moorwood, A. F. M., & Peletier, R. F. 1994, *A&A*, 288, 365
- Bono, G., Castellani, V., & Marconi, M. 2000, *ApJ*, 529, 293
- Bottinelli, L., Gouguenheim, L., Paturel, G., & de Vaucouleurs, G. 1985, *A&AS*, 59, 43
- Bouchet, P., Danziger, I. J., Gouiffes, C., della Valle, M., & Monetti, A. 1996, in *Supernovae and Supernova Remnants*, ed. R. McCray & Z. Wang (New York: Cambridge University Press), 201
- Buta, R., & de Vaucouleurs, G. 1983, *ApJS*, 51, 149
- Cardelli, J. A., Clayton, G. C., & Mathis, J. S. 1989, *ApJ*, 345, 245
- Castellanos, M., Díaz, A. I., & Terlevich, E. 2002, *MNRAS*, 329, 315
- Cousins, A. W. J. 1981, *South African Astronomical Observatory Circular*, 6, 4
- Danziger, I. J., Gouiffes, C., Bouchet, P., & Lucy, L. B. 1989, *IAU Circ.*, 4746, 1
- Dolphin, A. E. 2000, *PASP*, 112, 1383
- Eastman, R. G., & Kirshner, R. 1989, *ApJ*, 466, 911

- Eastman, R. G., & Pinto, P. A. 1993, *ApJ*, 412, 731
- Eastman, R. G., Schmidt, B. P., & Kirshner, R. 1996, *ApJ*, 466, 911 (E96)
- Eggleton, P. P. 1971, *MNRAS*, 151, 351
- . 1972, *MNRAS*, 156, 361
- . 1973, *MNRAS*, 163, 279
- Elmhamdi, A., et al. 2003, *MNRAS*, 338, 939
- Feast, M. 1999, *PASP*, 111, 775
- Filippenko, A. V. 1988, *AJ*, 96, 1941
- . 1997, *ARA&A*, 35, 309
- Freedman, W. L., et al. 1994, *ApJ*, 427, 628
- Freedman, W. L., et al. 2001, *ApJ*, 553, 47 (F01)
- Gibson, B. K., et al. 2000, *ApJ*, 529, 723
- Gieren, W. P., Fouquè, P., & Gómez, M. 1998, *ApJ*, 496, 17
- Graham, J. A., et al. 1997, *ApJ*, 477, 535
- Hamuy, M. 2001, Ph.D. thesis, The University of Arizona  
(available at <http://www.ociw.edu/~mhamuy>)
- . 2003, *ApJ*, 582, 905
- Hamuy, M., & Pinto, P. A. 2002, *ApJ*, 566, L63
- Hamuy, M., et al. 2001, *ApJ*, 558, 615
- Hamuy, M., & Suntzeff, N. B. 1990, *AJ*, 99, 1146
- Herrnstein, J. R., et al. 1999, *Nature*, 400, 539
- Höflich, P. 1991, *A&A*, 246, 481
- Holtzman, J. A., et al. 1995, *PASP*, 107, 156
- Johnson, H. L., Iriarte, B., Mitchell, R. I., & Wisniewskij, W. Z. 1966, *Communications of the Lunar and Planetary Laboratory*, 4, 99

- Kanbur, S. M., Iono, D., Tanvir, N. R., & Hendry, M. A. 2002, *MNRAS*, 329, 126
- Kanbur, S. M., Ngeow, C. C., Tanvir, N. R., & Hendry, M. A. 2003, *A&A*, submitted
- Kennicutt, R. C., et al. 1998, *ApJ*, 498, 181
- Kirshner, R. P., & Kwan, J. 1974, *ApJ*, 193, 27
- Kochanek, C. S. 1997, *ApJ*, 491, 13
- Krist, J. 1995, in *ASP Conf. Ser. 77: Astronomical Data Analysis Software and Systems IV*, ed. R.A. Shaw, H.E. Payne, & J.J.E. Hayes (San Francisco: ASP), 349
- Leonard, D. C., & Filippenko, A. V. 2001, *PASP*, 113, 920
- Leonard, D. C., Filippenko, A. V., Ardila, D. R., & Brotherton, M. S. 2001, *ApJ*, 553, 861
- Leonard, D. C., et al. 2002a, *PASP*, 114, 35
- Leonard, D. C., et al. 2002b, *AJ*, 124, 2490
- Leonard, D. C., Filippenko, A. V., & Matheson, T. 2000, in *Cosmic Explosions*, ed. S. S. Holt & W. W. Zhang (New York: AIP), 165
- Lucy, L. B. 1988, in *Supernova 1987A in the Large Magellanic Cloud*, ed. M. Kaplan & A. G. Michlitsianos (Cambridge: Cambridge University Press), 323
- Madore, B. F. 1982, *ApJ*, 253, 575
- Madore, B. F., & Freedman, W. L. 1991, *PASP*, 103, 933
- Meynet, G., Maeder, A., Schaller, G., Schaerer, D., & Charbonnel, C. 1994, *A&AS*, 103, 97
- Mitchell, R. C., Baron, E., Branch, D., Hauschildt, P. H., Nugent, P. E., Lundqvist, P., Blinnikov, S., & Pun, C. S. J. 2002, *ApJ*, 574, 293
- Moffett, T. J., & Barnes, T. G. 1984, *ApJS*, 55, 389
- Moffett, T. J., Gieren, W. P., Barnes, T. G., & Gómez, M. 1998, *ApJS*, 117, 135
- Montes, M. J., & Wagoner, R. V. 1995, *ApJ*, 445, 828
- Nadyozhin, D. K. 1998, in *Supernovae and Cosmology*, ed. L. Labhardt, B. Binggeli, & R. Buser (Basel: Astron. Inst. Univ. Basel), 125
- Nadyozhin, D. K. 2003, *MNRAS*, submitted (astro-ph/0303411)

- Newman, J. A., Ferrarese, L., Stetson, P. B., Maoz, E., Zepf, S. E., Davis, M., Freedman, W. L., & Madore, B. F. 2001, *ApJ*, 553, 562
- Ngeow, C. C., Kanbur, S. M., Nikolaev, S., Tanvir, N. R., & Hendry, M. A. 2003, *ApJ*, 586, 959
- Parodi, B. R., Saha, A., Sandage, A., & Tammann, G. A. 2000, *ApJ*, 540, 634
- Patat, F., Barbon, R., Cappellaro, E., & Turatto, M. 1993, *A&AS*, 98, 443
- . 1994, *A&A*, 282, 731
- Perlmutter, S., et al. 1999, *ApJ*, 517, 565
- Phillips, M. M. 1993, *ApJ*, 413, L105
- Pooley, D., et al. 2002, *ApJ*, 572, 932
- Riess, A. G., et al. 1998, *AJ*, 116, 1009
- Riess, A. G., Press, W. H., & Kirshner, R. P. 1996, *ApJ*, 473, 88
- Rozanski, R., & Rowan-Robinson, M. 1994, *MNRAS*, 271, 530
- Ryder, S. D., & Dopita, M. A. 1993, *ApJS*, 88, 415
- Saha, A., & Hoessel, J. G. 1990, *AJ*, 99, 97
- Saha, A., Labhardt, L., & Prosser, C. 2000, *PASP*, 112, 163
- Saha, A., Sandage, A., Tammann, G. A., Dolphin, A. E., Christensen, J., Panagia, N., & Macchetto, F. D. 2001a, *ApJ*, 562, 314
- Saha, A., Sandage, A., Thim, F., Labhardt, L., Tammann, G. A., Christensen, J., Panagia, N., & Macchetto, F. D. 2001b, *ApJ*, 551, 973
- Sandage, A. 1958, *ApJ*, 127, 513
- Sasselov, D. D., et al. 1997, *A&A*, 324, 471
- Schechter, P. L., Mateo, M., & Saha, A. 1993, *PASP*, 105, 1342
- Schlegel, E. M. 1990, *MNRAS*, 244, 269
- Schmidt, B. P., Kirshner, R. P., & Eastman, R. G. 1992, *ApJ*, 395, 366

- Schmidt, B. P., et al. 1993, *Nature*, 364, 600
- Schmidt, B. P., Kirshner, R. P., Eastman, R. G., Phillips, M. M., Suntzeff, N. B., Hamuy, M., Maza, J., & Aviles, R. 1994, *ApJ*, 432, 42
- Schmutz, W., Abbott, D. C., Russell, R. S., Hamann, W.-R., & Wessolowski, U. 1990, *ApJ*, 355, 255
- Sebo, K. M., et al. 2002, *ApJS*, 142, 71
- Smartt, S. J., Gilmore, G. F., Tout, C. A., & Hodgkin, S. T. 2002, *ApJ*, 565, 1089
- Sohn, Y., & Davidge, T. J. 1998, *AJ*, 115, 130
- Stetson, P. B. 1987, *PASP*, 99, 191
- . 1994, *PASP*, 106, 250
- Suntzeff, N. B., Phillips, M. M., Elias, J. H., Walker, A. R., & Depoy, D. L. 1992, *ApJ*, 384, L33
- Tammann, G. A., & Reindl, B. 2002a, *proc. XXXVIIth Moriond Astrophysics Meeting, The Cosmological Model*, in press (astro-ph/0208176)
- . 2002b, *Baltic Astronomy*, 11, 297 (T02)
- Tammann, G. A., Reindl, B., Thim, F., Saha, A., & Sandage, A. 2002, in *ASP Conf. Ser. 283, A New Era in Cosmology*, ed. N. Metcalfe & T. Shanks, in press (astro-ph/0112489)
- Tanvir, N. R. 1997, in *The Extragalactic Distance Scale*: ed. M. Livio (Cambridge: Cambridge University Press), 91
- . 1999, in *ASP Conf. Ser. 167: Harmonizing Cosmic Distance Scales in a Post-HIPPARCOS Era*, ed. D. Egret & A. Heck (San Francisco: ASP), 84
- Tanvir, N. R., & Boyle, A. 1999, *MNRAS*, 304, 957
- Tanvir, N. R., Ferguson, H. C., & Shanks, T. 1999, *MNRAS*, 310, 175
- Thim, F., Tammann, G. A., Saha, A., Dolphin, A., Sandage, A., Tolstoy, E., & Labhardt, L. 2003, *ApJ*, in press (astro-ph/0303101)
- Tonry, J. L., Blakeslee, J. P., Ajhar, E. A., & Dressler, A. 2000, *ApJ*, 530, 625

- Udalski, A., Szymanski, M., Kubiak, M., Pietrzynski, G., Soszynski, I., Wozniak, P., & Zebrun, K. 1999, *Acta Astronomica*, 49, 201
- van Zee, L., Salzer, J. J., Haynes, M. P., O'Donoghue, A. A., & Balonek, T. J. 1998, *AJ*, 116, 2805
- Wagoner, R. V. 1982, in *NATO ASIC Proc. 90: Supernovae: A Survey of Current Research*, ed. M. J. Rees & R. J. Stoneham (Dordrecht: Reidel), 253
- Woosley, S. E. 1988, *ApJ*, 330, 218
- Woosley, S. E., Pinto, P. A., Martin, P. G., & Weaver, T. A. 1987, *ApJ*, 318, 664
- Woosley, S. E., & Weaver, T. A. 1986, *ARA&A*, 24, 205

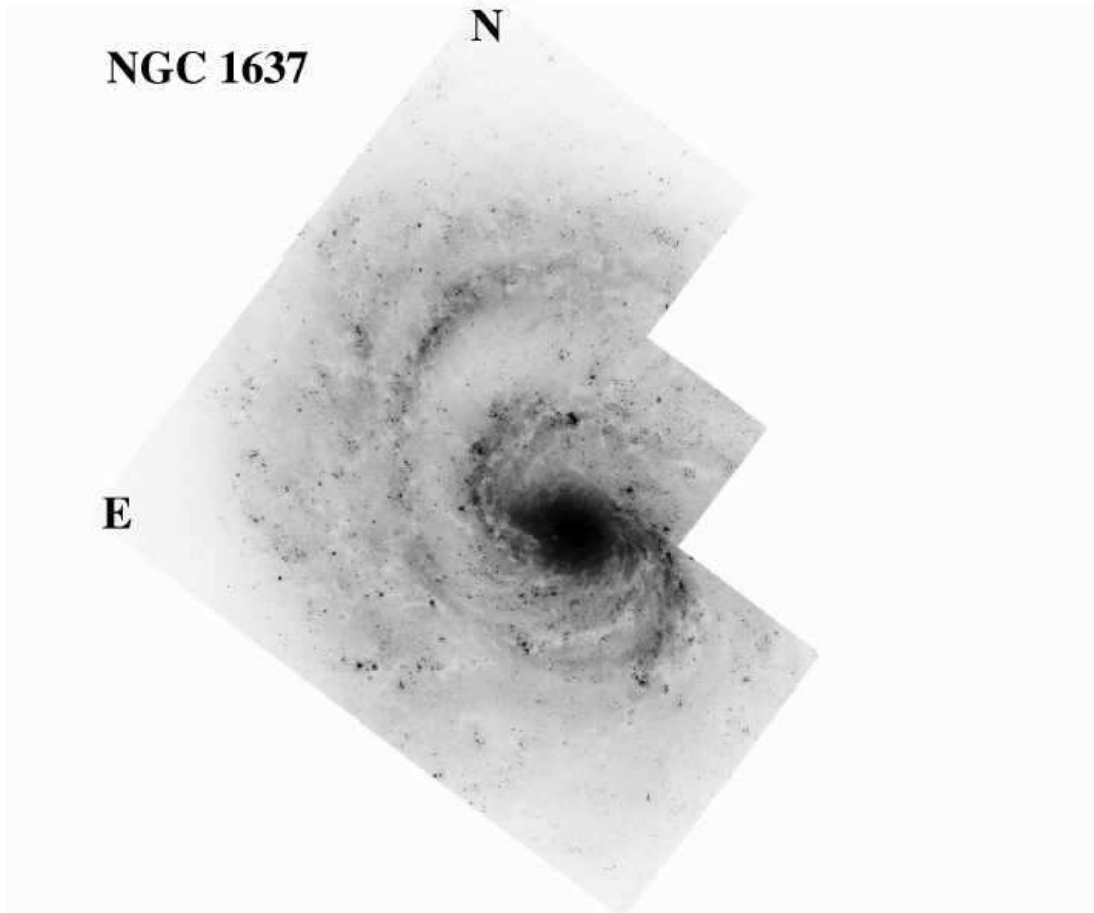


Fig. 1.— Mosaic of the NGC 1637 field produced by co-adding all *HST* WFPC2 images obtained with the F555W filter (*V*-band). The image has been rotated so that North is up and East is to the left, as indicated. The PC chip covers the smallest field (chip 1). Moving counterclockwise, the other three WF2 fields correspond to chips 2, 3, and 4.

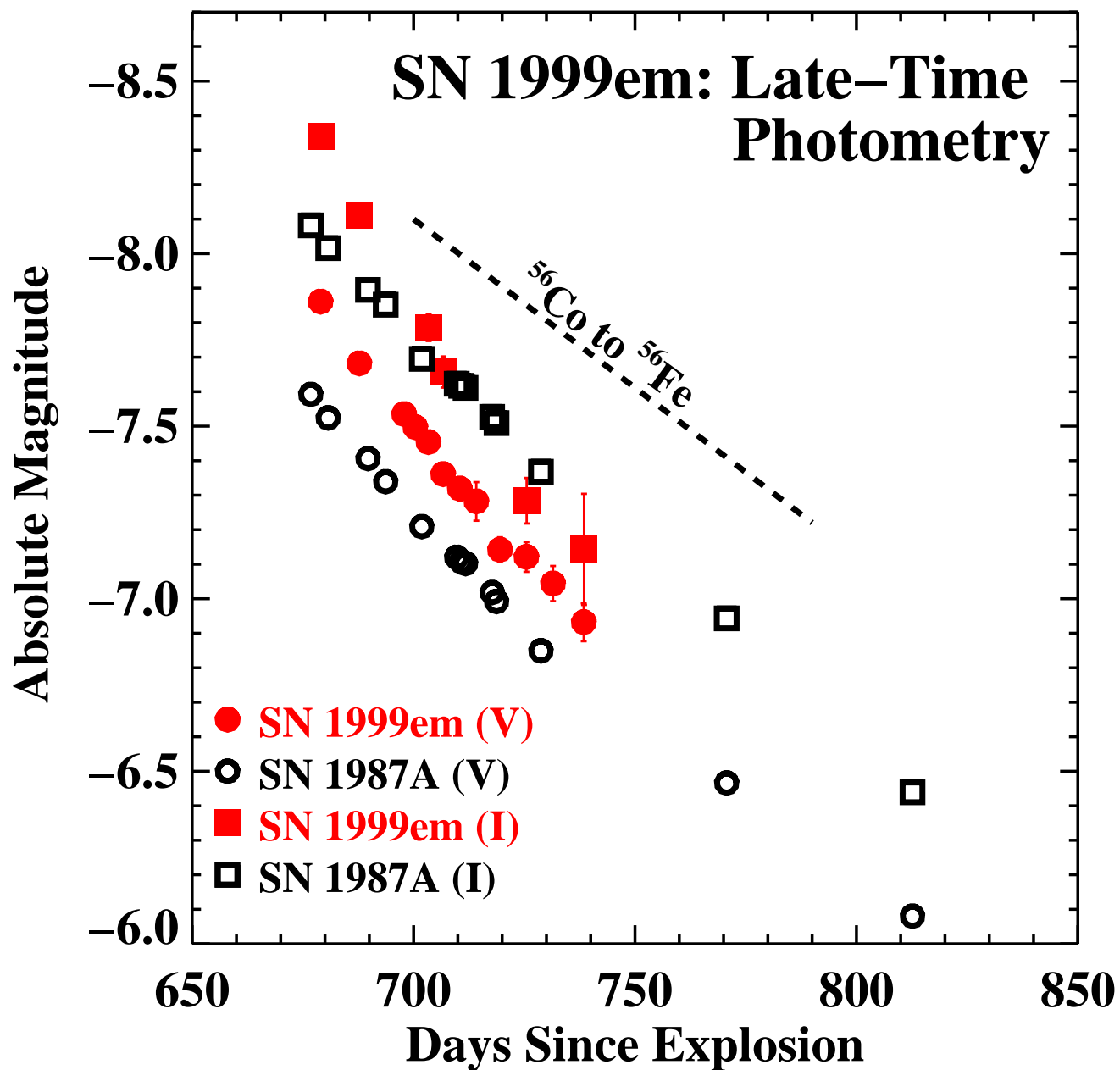


Fig. 2.— Photometric behavior of SN 1999em (*closed, red symbols*) compared with SN 1987A (*open, black symbols*) at  $\sim 2$  years after explosion. The fact that the optical and near-infrared brightnesses of both SNe decline substantially faster than the rate predicted by the radioactive decay of  $^{56}\text{Co}$  (*dashed line*) is attributed to increased envelope transparency to gamma rays and to dust formation in the cooling SN atmospheres; see text for details.

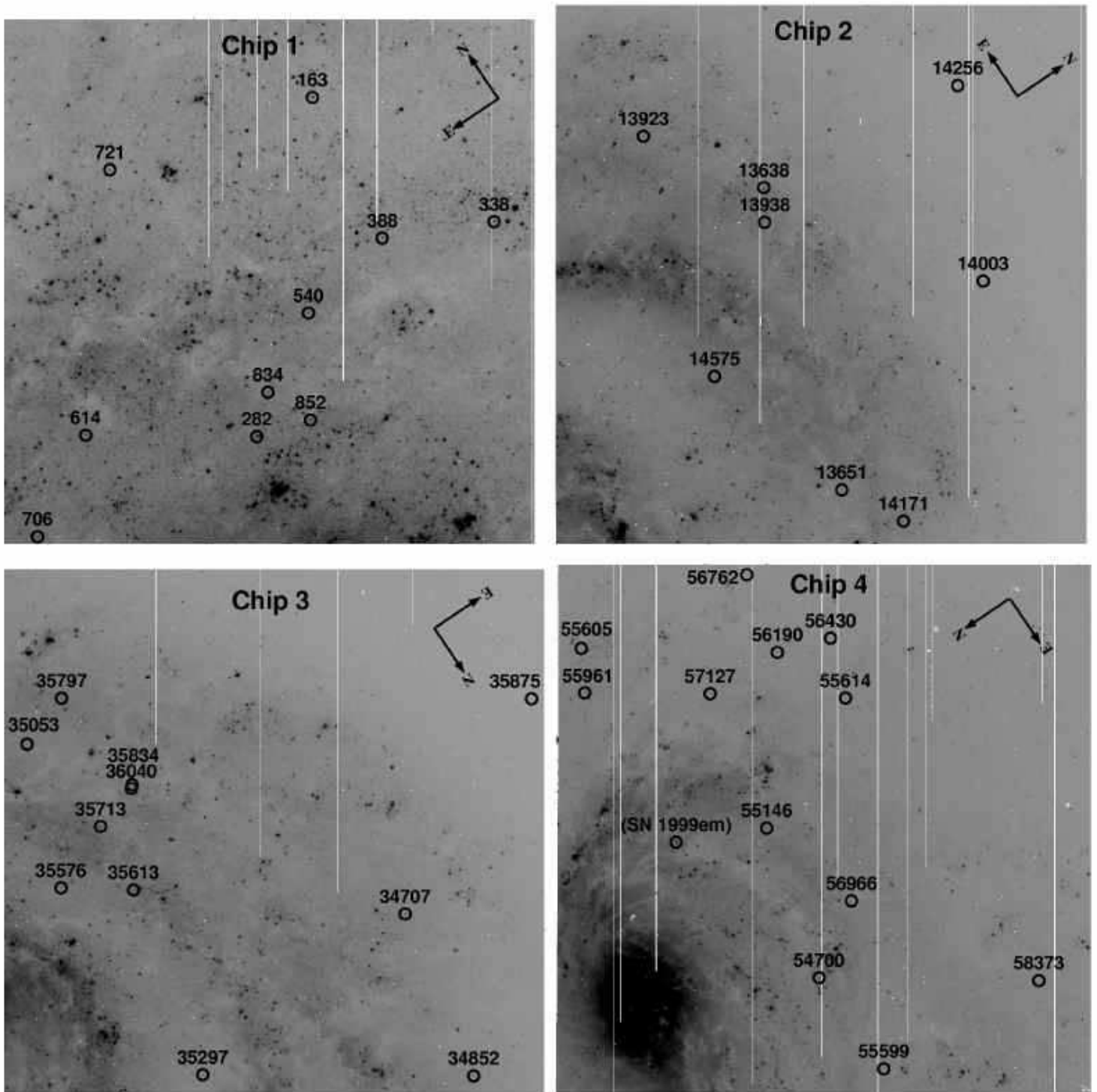


Fig. 3.— Finding charts for the NGC 1637 Cepheids on the four WFPC2 chips, from the combined  $V$ -band image. The Cepheids are circled and labeled with their identification number from Table 6. Masked pixels are white. The field of view is  $35'' \times 35''$  for chip 1 (Planetary Camera of the WFPC2), and  $1/3 \times 1/3$  chips 2, 3, and 4 (Wide Field Camera). SN 1999em is also labeled on chip 4 (*hstphot* object number 54475, located at pixel position  $X=213.1, Y=407.8$ ).

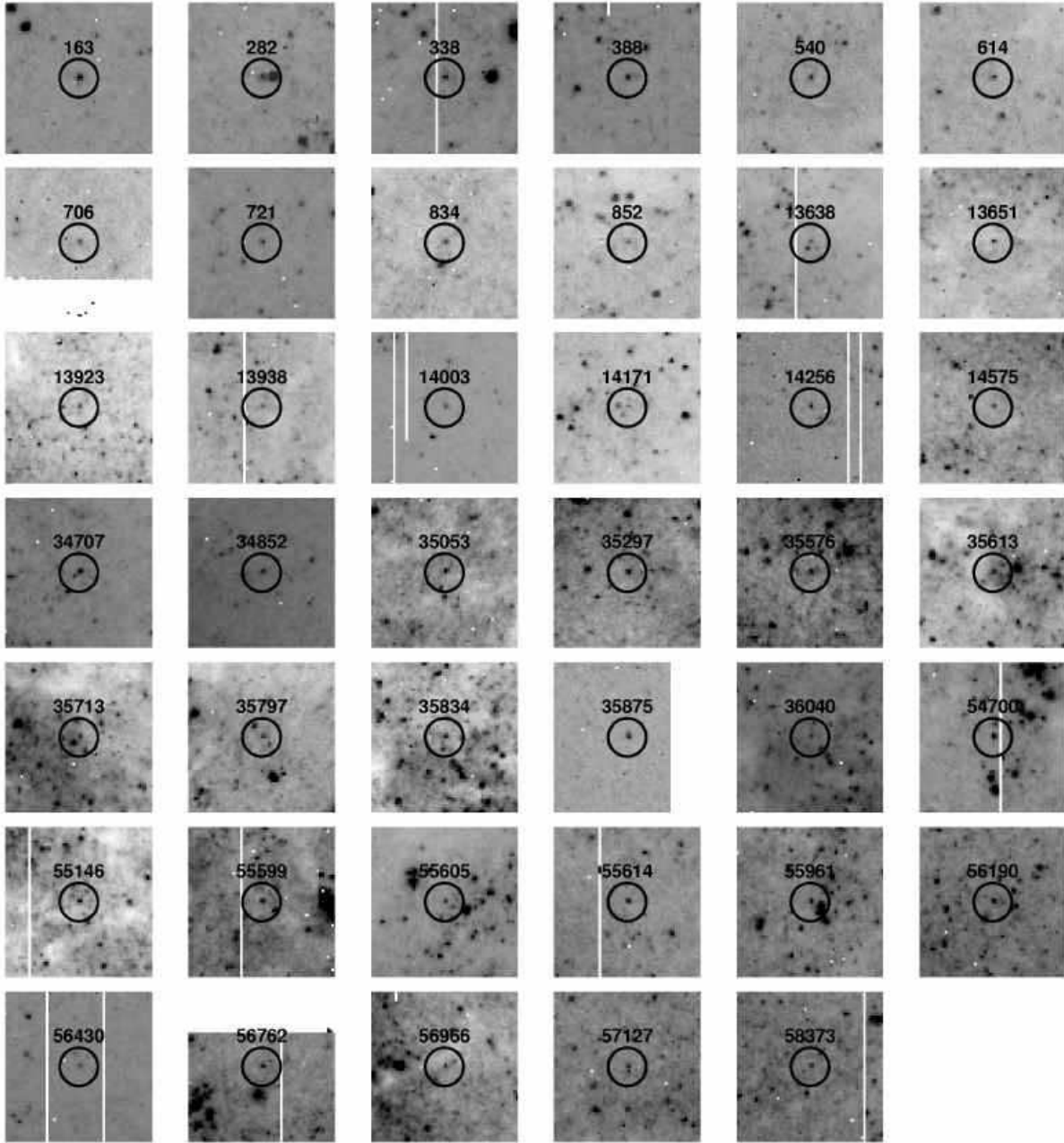


Fig. 4.— Close-up finder charts for the NGC 1637 Cepheids, with the contrast individually scaled to clearly show the candidate. Each panel is a  $60 \times 60$  pixel field of view centered on the variable.

Fig. 5.— Light curves of candidate Cepheids folded at the most likely period. The relative likelihoods (§ 4.4) of the best-fitting template light curves for periods between 10 and 100 days are also shown.

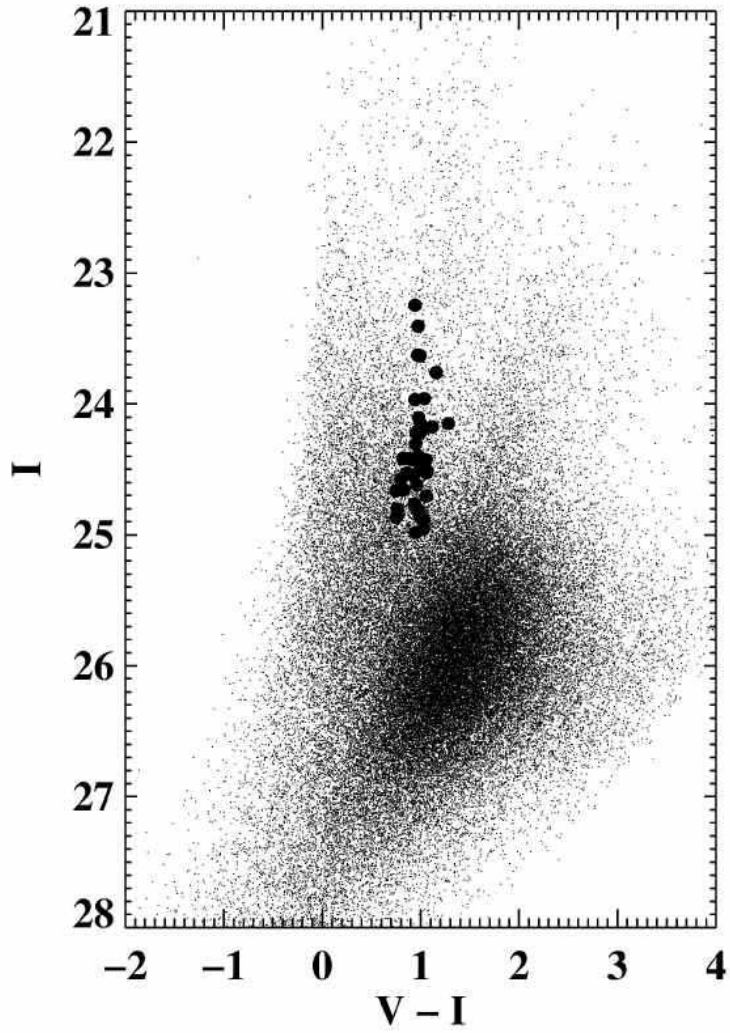


Fig. 6.— Color-magnitude diagram of all of the stars in the NGC 1637 field, with Cepheids indicated by *large closed circles*.

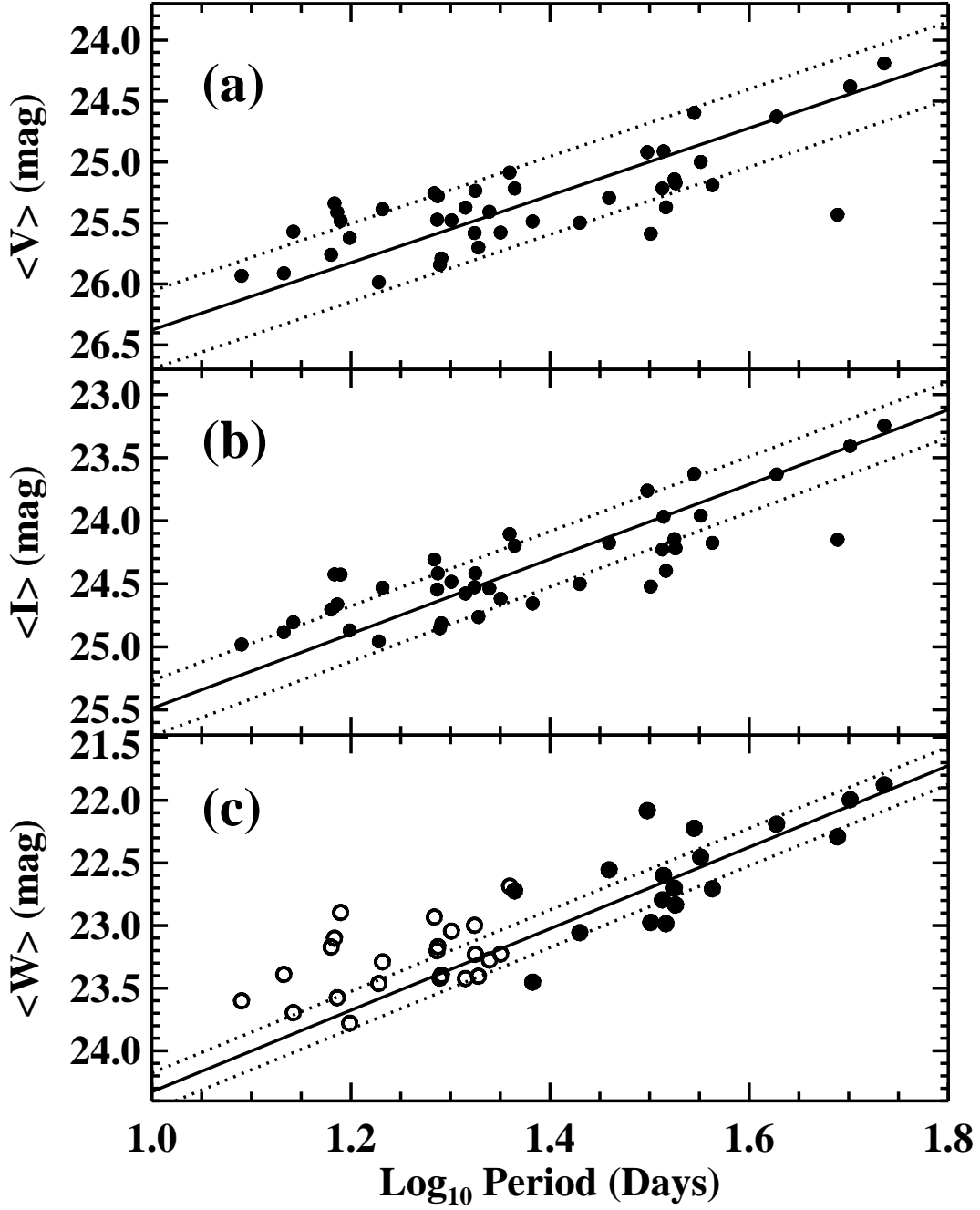


Fig. 7.— (a) Apparent  $V$ -band PL relation for the 41 Cepheids listed in Table 8. The solid line shows a least-squares fit to all data points, with the slope fixed to be that of the LMC PL relation adopted by the KP (eq. [17]). Dotted lines represent the expected intrinsic  $2\sigma$  scatter around the best fitting PL relation derived from the OGLE LMC Cepheids. (b) As in (a), except for the  $I$ -band. (c) As in (a), except for the “reddening-free”  $W$ -band, with Cepheids eliminated by the lower period cut described in the text indicated by *open circles*. The solid line shows a least-squares fit to the data points represented by the *closed circles*, with the slope fixed to be that of the LMC PL relation adopted by the KP (eq. [18]).

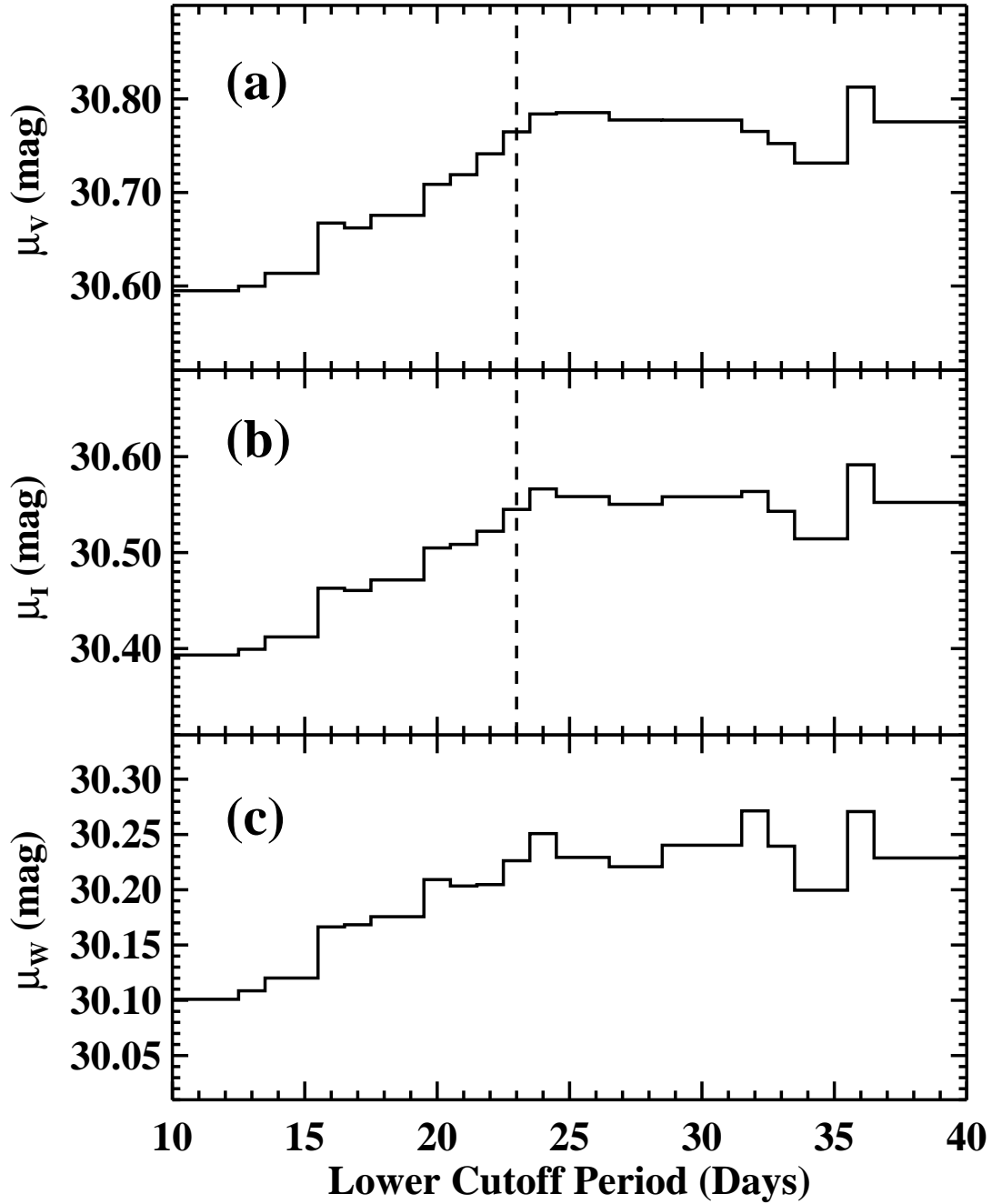


Fig. 8.— Distance modulus as a function of lower cutoff period for (a)  $V$ -band, (b)  $I$ -band, and (c)  $W$ -band. The *vertical dashed lines* in (a) and (b) indicate the point at which the apparent distance moduli stabilize, thereby defining the lower period cutoff threshold of 23.0 days. See text for details.

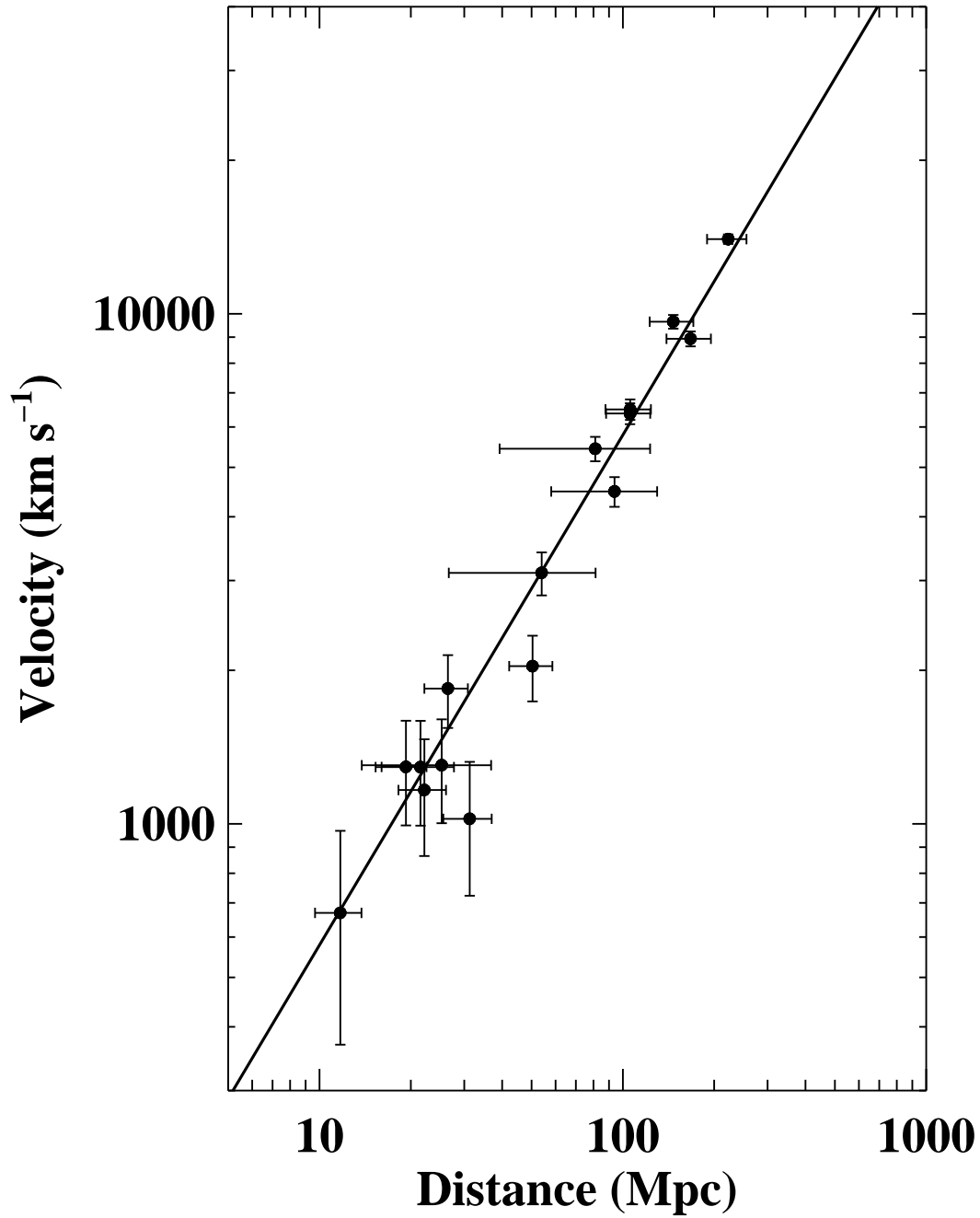


Fig. 9.— *V*-band Hubble diagram for the standard-candle method of Hamuy & Pinto (2002), as calibrated by the Cepheid distance to NGC 1637 derived in this paper.

Table 1. Slopes and Zero-Points for Cepheid PL Relations

Set	$a_V$	$a_I$	$a_W$	$b_V$	$b_I$	$b_W$	Reference
A	-2.760	-2.962	-3.255	-1.458	-1.942	-2.644	1
B	-2.760	-3.060	-3.495	-1.400	-1.810	-2.405	2
C	-2.480	-2.820	-3.313	-1.750	-2.090	-2.583	3
D	-3.140	-3.410	-3.802	-0.830	-1.330	-2.055	3

Note. — Slopes and zero points for the PL relations resulting from the four samples of Cepheids described in § 2.1. The relations are defined by  $M_C = a_C \log(P) + b_C$ , with  $M_C$  the absolute magnitude of a Cepheid in photometric band  $C$ ,  $P$  its period (usually measured in days), and  $a_C$  and  $b_C$  the slope and zero-point, respectively, of the relation.  $W$  represents the Weisenheit reddening-free index described in the text.

References. — (1) F01; (2) Madore & Freedman 1991; (3) Thim et al. 2003.

Table 2. Sources of Systematic Uncertainty in the Cepheid Distance to NGC 1637

Source of Uncertainty	Error (mag)
Zero-point of PL relations	0.10
Metallicity	0.12
Slope of PL relations	0.06
Aperture corrections	0.02
WFPC2 zero-point	0.04
Total systematic uncertainty	0.17

Table 3. *HST* Observations of NGC 1637

Epoch	Data Archive Designation	UT Date	HJD at Midexposure	Relative Day <sup>a</sup>	Exposure Time (s)
F555W					
1	u6fv0101/2m	2001 Sep 02	2452154.637	0.000	1100 + 1100
2	u6fv0201/2r	2001 Sep 10	2452163.395	8.759	1100 + 1100
3	u6fv0301/2m	2001 Sep 20	2452173.494	18.857	1100 + 1100
4	u6fv0401/2m	2001 Sep 23	2452176.029	21.392	1100 + 1100
5	u6fv0501/2m	2001 Sep 26	2452178.975	24.338	1100 + 1100
6	u6fv0601/2m	2001 Sep 29	2452182.319	27.682	1100 + 1100
7	u6fv0701/2m	2001 Oct 03	2452186.061	31.425	1100 + 1100
8	u6fv0801/2m	2001 Oct 07	2452189.804	35.167	1100 + 1100
9	u6fv0901/2m	2001 Oct 12	2452195.152	40.515	1100 + 1100
10	u6fv1001/2m	2001 Oct 18	2452201.105	46.469	1100 + 1100
11	u6fv1101/2m	2001 Oct 24	2452207.117	52.481	1100 + 1100
12	u6fv1201/2m	2001 Oct 31	2452214.071	59.434	1100 + 1100
F814W					
1	u6fv0103/4m	2001 Sep 02	2452154.699	0.000	1100 + 1100
2	u6fv0203/4r	2001 Sep 10	2452163.458	8.759	1100 + 1100
5	u6fv0503/4m	2001 Sep 26	2452179.041	24.342	1100 + 1100
6	u6fv0603/4m	2001 Sep 29	2452182.381	27.682	1100 + 1100
10	u6fv1003/4m	2001 Oct 18	2452201.168	46.469	1100 + 1100
12	u6fv1203/4m	2001 Oct 31	2452214.137	59.438	1100 + 1100

<sup>a</sup>Day since first epoch in each filter.

Table 4. Reference Star Photometry

ID	Chip	$X$	$Y$	$V$	$I$
16	1	507.7	195.9	$22.87 \pm 0.00$	$21.95 \pm 0.01$
49	1	170.6	700.8	$23.50 \pm 0.01$	$23.07 \pm 0.01$
52	1	599.6	120.7	$23.50 \pm 0.01$	$23.22 \pm 0.02$
94	1	258.4	543.1	$23.91 \pm 0.01$	$23.78 \pm 0.02$
12912	2	117.1	64.4	$22.72 \pm 0.00$	$22.44 \pm 0.01$
12929	2	196.8	717.9	$22.82 \pm 0.00$	$22.79 \pm 0.01$
12932	2	331.0	583.5	$23.09 \pm 0.00$	$22.55 \pm 0.01$
12935	2	226.1	384.5	$23.00 \pm 0.00$	$22.97 \pm 0.01$
12955	2	514.1	196.7	$23.39 \pm 0.01$	$22.78 \pm 0.01$
12967	2	270.9	69.3	$23.53 \pm 0.01$	$22.83 \pm 0.01$
13022	2	352.9	149.2	$23.88 \pm 0.01$	$23.38 \pm 0.02$
13035	2	373.8	291.3	$23.95 \pm 0.01$	$23.48 \pm 0.02$
34397	3	257.5	154.6	$22.85 \pm 0.00$	$22.55 \pm 0.01$
34410	3	241.7	607.9	$23.08 \pm 0.00$	$22.38 \pm 0.01$
34420	3	210.6	310.5	$23.37 \pm 0.01$	$21.96 \pm 0.01$
34455	3	397.0	258.3	$23.23 \pm 0.01$	$23.27 \pm 0.02$
34493	3	231.3	568.2	$23.59 \pm 0.01$	$23.47 \pm 0.02$
34510	3	665.5	332.5	$23.63 \pm 0.01$	$23.78 \pm 0.03$
34547	3	359.8	569.8	$23.69 \pm 0.01$	$23.74 \pm 0.02$
34586	3	278.7	339.1	$23.97 \pm 0.01$	$23.70 \pm 0.03$
34598	3	145.4	244.5	$23.93 \pm 0.01$	$23.84 \pm 0.03$
54399	4	545.7	680.5	$22.24 \pm 0.00$	$21.63 \pm 0.01$
54445	4	121.4	526.4	$23.25 \pm 0.00$	$21.68 \pm 0.00$
54478	4	330.6	227.4	$23.13 \pm 0.00$	$23.02 \pm 0.01$
54506	4	166.6	681.4	$23.41 \pm 0.01$	$22.88 \pm 0.01$
54516	4	290.1	87.2	$23.67 \pm 0.01$	$22.34 \pm 0.01$
54560	4	208.2	313.0	$23.65 \pm 0.01$	$23.25 \pm 0.02$
54567	4	671.8	284.6	$23.61 \pm 0.01$	$23.40 \pm 0.02$
54587	4	127.3	471.3	$23.75 \pm 0.01$	$23.40 \pm 0.03$
54594	4	247.5	488.5	$23.76 \pm 0.01$	$23.22 \pm 0.02$
54598	4	374.3	184.1	$23.77 \pm 0.01$	$23.28 \pm 0.02$
54626	4	350.5	555.4	$23.81 \pm 0.01$	$23.55 \pm 0.02$
54641	4	73.5	419.8	$23.94 \pm 0.01$	$23.69 \pm 0.03$
54684	4	766.5	379.5	$23.97 \pm 0.01$	$23.70 \pm 0.02$
54692	4	66.6	692.6	$23.94 \pm 0.01$	$24.01 \pm 0.03$
54709	4	396.2	416.7	$23.96 \pm 0.01$	$23.89 \pm 0.03$
54725	4	507.7	268.3	$23.96 \pm 0.01$	$24.12 \pm 0.03$

Note. — Photometry of bright, non-variable stars in NGC 1637. Uncertainties are the formal photometric errors reported by *hstphot* for measurements made on the combined  $V$  (12 epochs) and  $I$  (6 epochs) frames. Note that formal uncertainties that are less than 0.005 mag are reported here as 0.00 mag.

Table 5. Photometry of SN 1999em

Epoch <sup>a</sup>	Day <sup>b</sup>	$V$ ( $\sigma_V$ )	$I$ ( $\sigma_I$ )
1	679	22.791 (0.016)	22.187 (0.021)
2	688	22.970 (0.017)	22.415 (0.023)
3	698	23.117 (0.022)	...
4	700	23.155 (0.027)	...
5	703	23.198 (0.030)	22.740 (0.039)
6	707	23.291 (0.027)	22.869 (0.045)
7	710	23.333 (0.034)	...
8	714	23.370 (0.056)	...
9	720	23.510 (0.036)	...
10	725	23.531 (0.043)	23.242 (0.066)
11	731	23.608 (0.051)	...
12	738	23.720 (0.055)	23.383 (0.161)

<sup>a</sup>As defined by Table 3.

<sup>b</sup>Day since estimated explosion date of HJD 2,451,475.64 (Leonard et al. 2002a).

Table 6. Coordinates of Cepheid Variables in NGC 1637

ID	Chip	X	Y
163	1	485.9	688.5
282	1	407.6	210.8
338	1	742.1	513.5
388	1	584.5	490.2
540	1	480.4	384.6
614	1	166.2	212.5
706	1	98.2	69.3
721	1	200.2	586.6
834	1	423.3	273.0
852	1	483.2	233.8
13638	2	342.8	533.3
13651	2	452.9	107.3
13923	2	173.2	605.8
13938	2	344.0	484.7
14003	2	652.3	401.9
14171	2	540.0	63.3
14256	2	616.5	677.3
14575	2	273.3	267.3
34707	3	602.7	312.7
34852	3	699.3	84.4
35053	3	68.4	550.8
35297	3	317.2	86.0
35576	3	117.2	349.2
35613	3	219.7	346.3
35713	3	173.1	435.9
35797	3	117.9	616.8
35834	3	217.7	494.6
35875	3	781.0	615.9
36040	3	216.5	489.3
54700	4	414.8	216.8
55146	4	341.1	427.5
55599	4	506.2	88.4
55605	4	79.3	680.9
55614	4	452.2	610.9
55961	4	84.4	618.1
56190	4	356.1	675.1
56430	4	430.9	695.4
56762	4	313.0	784.7
56966	4	460.6	325.1
57127	4	261.3	616.8
58373	4	724.9	212.8

Table 7. Photometry of Cepheid Variables in NGC 1637

Epoch	V	I	V	I	V	I	V	I
	163		282		338		388	
1	24.83 ± 0.08	23.82 ± 0.08	24.68 ± 0.07	23.77 ± 0.08	24.86 ± 0.06	23.92 ± 0.06	24.82 ± 0.09	23.93 ± 0.07
2	25.13 ± 0.08	24.00 ± 0.06	25.01 ± 0.08	23.90 ± 0.07	24.93 ± 0.07	23.97 ± 0.06	25.33 ± 0.08	24.22 ± 0.08
3	24.10 ± 0.03	...	25.58 ± 0.10	...	25.42 ± 0.10	...	25.72 ± 0.12	...
4	24.28 ± 0.05	...	25.55 ± 0.11	...	25.64 ± 0.12	...	25.63 ± 0.10	...
5	24.33 ± 0.05	23.43 ± 0.08	25.31 ± 0.08	24.34 ± 0.09	25.53 ± 0.10	24.47 ± 0.10	25.75 ± 0.10	24.63 ± 0.10
6	24.55 ± 0.05	23.50 ± 0.04	24.91 ± 0.06	23.90 ± 0.08	25.49 ± 0.11	24.54 ± 0.10	25.04 ± 0.06	24.18 ± 0.08
7	24.74 ± 0.05	...	24.49 ± 0.05	...	25.39 ± 0.09	...	24.61 ± 0.06	...
8	24.78 ± 0.09	...	24.65 ± 0.06	...	24.59 ± 0.04	...	24.99 ± 0.06	...
9	25.03 ± 0.06	...	24.93 ± 0.06	...	24.81 ± 0.05	...	25.05 ± 0.13	...
10	25.14 ± 0.07	23.94 ± 0.10	25.15 ± 0.10	24.01 ± 0.09	25.18 ± 0.07	24.02 ± 0.10	25.22 ± 0.12	24.16 ± 0.07
11	24.02 ± 0.04	...	25.32 ± 0.14	...	25.36 ± 0.08	...	25.58 ± 0.10	...
12	24.35 ± 0.04	23.45 ± 0.06	25.47 ± 0.11	24.33 ± 0.11	25.68 ± 0.13	24.63 ± 0.11	25.62 ± 0.10	24.41 ± 0.11
	540		614		706		721	
1	26.11 ± 0.16	25.19 ± 0.19	25.65 ± 0.10	24.74 ± 0.12	25.15 ± 0.09	24.68 ± 0.16	26.10 ± 0.15	24.99 ± 0.15
2	25.37 ± 0.08	24.27 ± 0.08	25.87 ± 0.11	24.83 ± 0.12	25.91 ± 0.13	24.84 ± 0.15	25.31 ± 0.07	24.65 ± 0.11
3	26.05 ± 0.12	...	25.42 ± 0.09	...	25.30 ± 0.08	...	25.98 ± 0.12	...
4	26.00 ± 0.16	...	25.70 ± 0.12	...	25.45 ± 0.10	...	26.19 ± 0.14	...
5	25.84 ± 0.11	25.05 ± 0.17	25.77 ± 0.15	25.09 ± 0.16	25.83 ± 0.15	24.93 ± 0.13	26.10 ± 0.15	24.94 ± 0.14
6	24.90 ± 0.05	24.35 ± 0.09	25.70 ± 0.11	24.80 ± 0.11	26.04 ± 0.13	24.66 ± 0.13	25.62 ± 0.11	24.66 ± 0.10
7	25.17 ± 0.08	...	25.35 ± 0.09	...	26.48 ± 0.30	...	25.29 ± 0.07	...
8	25.40 ± 0.09	...	25.66 ± 0.10	...	26.11 ± 0.14	...	25.55 ± 0.09	...
9	25.89 ± 0.14	...	25.80 ± 0.10	...	25.36 ± 0.11	...	26.14 ± 0.13	...
10	25.99 ± 0.13	25.05 ± 0.15	25.33 ± 0.07	24.74 ± 0.11	25.88 ± 0.14	24.68 ± 0.14	25.92 ± 0.12	25.11 ± 0.19
11	24.78 ± 0.05	...	25.91 ± 0.13	...	26.63 ± 0.25	...	25.33 ± 0.08	...
12	25.50 ± 0.08	24.58 ± 0.14	25.32 ± 0.07	24.67 ± 0.11	25.35 ± 0.09	24.47 ± 0.12	25.77 ± 0.10	24.76 ± 0.13
	834		852		13638		13651	
1	26.72 ± 0.26	24.97 ± 0.18	25.91 ± 0.12	24.79 ± 0.15	25.00 ± 0.09	24.68 ± 0.11	25.12 ± 0.08	23.98 ± 0.06
2	25.80 ± 0.15	24.72 ± 0.18	25.75 ± 0.13	24.94 ± 0.18	25.41 ± 0.13	24.43 ± 0.09	25.70 ± 0.11	24.49 ± 0.12
3	25.34 ± 0.07	...	26.52 ± 0.25	...	25.46 ± 0.09	...	26.14 ± 0.14	...
4	25.43 ± 0.16	...	25.44 ± 0.08	...	24.86 ± 0.05	...	24.75 ± 0.06	...
5	25.99 ± 0.12	25.09 ± 0.15	25.68 ± 0.12	24.66 ± 0.14	25.02 ± 0.07	24.06 ± 0.10	24.70 ± 0.05	23.84 ± 0.06
6	26.88 ± 0.26	24.92 ± 0.15	26.40 ± 0.17	25.14 ± 0.19	25.27 ± 0.08	24.38 ± 0.08	24.96 ± 0.06	23.86 ± 0.16
7	26.04 ± 0.12	...	26.45 ± 0.20	...	25.66 ± 0.12	...	25.23 ± 0.08	...
8	25.79 ± 0.10	...	25.45 ± 0.09	...	25.58 ± 0.12	...	25.57 ± 0.11	...
9	26.23 ± 0.14	...	26.71 ± 0.25	...	24.67 ± 0.05	...	25.67 ± 0.10	...
10	25.44 ± 0.08	24.66 ± 0.11	25.34 ± 0.08	24.76 ± 0.17	25.47 ± 0.09	24.39 ± 0.12	25.93 ± 0.19	24.68 ± 0.10
11	26.23 ± 0.17	...	26.47 ± 0.21	...	25.61 ± 0.09	...	24.75 ± 0.05	...
12	25.44 ± 0.08	24.71 ± 0.12	25.44 ± 0.10	24.83 ± 0.22	24.80 ± 0.05	24.09 ± 0.06	25.25 ± 0.07	23.98 ± 0.06
	13923		13938		14003		14171	
1	25.84 ± 0.16	24.73 ± 0.32	25.43 ± 0.09	24.45 ± 0.09	25.72 ± 0.09	24.64 ± 0.11	25.61 ± 0.18	24.58 ± 0.14
2	25.72 ± 0.13	24.53 ± 0.10	25.75 ± 0.17	25.04 ± 0.15	25.50 ± 0.08	24.49 ± 0.09	26.56 ± 0.39	24.97 ± 0.16
3	25.11 ± 0.07	...	24.75 ± 0.09	...	24.84 ± 0.19	...	25.16 ± 0.09	...
4	25.37 ± 0.09	...	25.33 ± 0.09	...	25.22 ± 0.06	...	25.31 ± 0.09	...
5	25.23 ± 0.08	24.36 ± 0.09	25.39 ± 0.29	24.39 ± 0.09	25.62 ± 0.08	24.38 ± 0.07	25.62 ± 0.11	24.37 ± 0.09
6	25.47 ± 0.13	24.38 ± 0.09	26.11 ± 0.37	24.87 ± 0.54	25.76 ± 0.10	24.90 ± 0.11	25.86 ± 0.13	24.91 ± 0.16
7	25.77 ± 0.12	...	25.74 ± 0.12	...	25.39 ± 0.09	...	25.64 ± 0.16	...
8	26.31 ± 0.20	...	25.71 ± 0.11	...	24.99 ± 0.07	...	26.12 ± 0.16	...
9	25.91 ± 0.17	...	25.08 ± 0.08	...	25.53 ± 0.10	...	25.01 ± 0.09	...
10	24.81 ± 0.06	24.13 ± 0.08	25.54 ± 0.09	24.57 ± 0.26	25.44 ± 0.08	24.68 ± 0.11	25.24 ± 0.10	24.39 ± 0.09
11	25.13 ± 0.08	...	26.09 ± 0.15	...	25.20 ± 0.07	...	25.94 ± 0.19	...
12	25.56 ± 0.11	24.49 ± 0.12	24.86 ± 0.06	24.18 ± 0.18	25.62 ± 0.22	24.93 ± 0.15	25.88 ± 0.14	24.75 ± 0.11
	14256		14575		34707		34852	
1	25.58 ± 0.08	24.87 ± 0.12	25.40 ± 0.08	25.08 ± 0.25	24.35 ± 0.04	23.39 ± 0.04	24.30 ± 0.04	23.52 ± 0.05
2	25.89 ± 0.13	24.75 ± 0.09	26.26 ± 0.18	25.22 ± 0.27	24.66 ± 0.05	23.54 ± 0.05	24.71 ± 0.06	23.49 ± 0.05
3	25.94 ± 0.11	...	25.44 ± 0.08	...	24.97 ± 0.06	...	25.13 ± 0.08	...
4	...	...	25.66 ± 0.11	...	24.91 ± 0.06	...	25.16 ± 0.07	...
5	26.01 ± 0.18	25.12 ± 0.15	25.80 ± 0.11	24.67 ± 0.15	24.56 ± 0.05	23.62 ± 0.05	25.16 ± 0.07	24.07 ± 0.08
6	25.13 ± 0.06	24.75 ± 0.11	26.17 ± 0.19	...	24.15 ± 0.04	23.22 ± 0.04	25.09 ± 0.08	24.15 ± 0.11
7	25.32 ± 0.06	...	26.31 ± 0.25	...	23.78 ± 0.06	...	24.56 ± 0.05	...
8	26.01 ± 0.14	...	25.80 ± 0.27	...	24.06 ± 0.03	...	24.12 ± 0.03	...
9	25.79 ± 0.10	...	25.67 ± 0.11	...	24.18 ± 0.04	...	24.24 ± 0.04	...
10	25.33 ± 0.07	24.71 ± 0.11	26.32 ± 0.17	24.84 ± 0.17	24.31 ± 0.04	23.29 ± 0.04	24.51 ± 0.06	23.48 ± 0.04
11	25.97 ± 0.11	...	26.27 ± 0.16	...	24.40 ± 0.04	...	24.62 ± 0.07	...
12	25.16 ± 0.06	24.52 ± 0.08	25.47 ± 0.08	24.59 ± 0.14	24.76 ± 0.05	23.54 ± 0.05	25.05 ± 0.06	23.85 ± 0.08

Table 7—Continued

Epoch	<i>V</i>	<i>I</i>	<i>V</i>	<i>I</i>	<i>V</i>	<i>I</i>	<i>V</i>	<i>I</i>
	35053		35297		35576		35613	
1	25.55 ± 0.12	24.06 ± 0.08	25.35 ± 0.20	24.13 ± 0.08	25.56 ± 0.32	24.51 ± 0.14	25.17 ± 0.11	24.52 ± 0.14
2	25.27 ± 0.09	24.01 ± 0.07	25.37 ± 0.15	24.31 ± 0.10	25.52 ± 0.15	24.42 ± 0.13	25.62 ± 0.13	24.65 ± 0.19
3	24.72 ± 0.06	...	24.94 ± 0.06	...	25.26 ± 0.09	...	25.34 ± 0.09	...
4	24.78 ± 0.07	...	25.09 ± 0.07	...	25.36 ± 0.09	...	25.20 ± 0.08	...
5	25.02 ± 0.10	23.78 ± 0.07	25.27 ± 0.09	24.29 ± 0.08	25.89 ± 0.14	24.07 ± 0.14	25.36 ± 0.09	24.39 ± 0.10
6	25.11 ± 0.08	23.81 ± 0.06	25.36 ± 0.09	24.36 ± 0.09	25.78 ± 0.13	24.64 ± 0.15	25.53 ± 0.14	24.77 ± 0.14
7	25.19 ± 0.09	...	25.86 ± 0.12	...	25.50 ± 0.12	...	25.40 ± 0.10	...
8	25.31 ± 0.10	...	24.72 ± 0.05	...	24.63 ± 0.05	...	24.70 ± 0.06	...
9	25.14 ± 0.09	...	24.78 ± 0.05	...	25.07 ± 0.08	...	25.25 ± 0.09	...
10	24.43 ± 0.05	23.45 ± 0.05	25.45 ± 0.12	24.24 ± 0.08	25.70 ± 0.14	24.48 ± 0.12	25.70 ± 0.13	24.85 ± 0.24
11	24.82 ± 0.07	...	25.75 ± 0.12	...	25.59 ± 0.10	...	25.70 ± 0.12	...
12	25.24 ± 0.09	23.99 ± 0.08	24.52 ± 0.04	23.72 ± 0.12	24.51 ± 0.13	23.93 ± 0.06	24.59 ± 0.27	24.17 ± 0.08
	35713		35797		35834		35875	
1	26.27 ± 0.26	24.74 ± 0.33	25.67 ± 0.14	25.46 ± 0.34	25.24 ± 0.14	24.46 ± 0.13	26.15 ± 0.19	25.14 ± 0.20
2	25.39 ± 0.13	24.59 ± 0.35	25.01 ± 0.08	23.88 ± 0.11	25.80 ± 0.15	24.61 ± 0.31	25.21 ± 0.12	24.52 ± 0.08
3	25.69 ± 0.17	...	25.64 ± 0.13	...	25.09 ± 0.08	...	25.94 ± 0.12	...
4	25.49 ± 0.11	...	25.94 ± 0.16	...	25.33 ± 0.13	...	25.05 ± 0.10	...
5	24.74 ± 0.10	24.31 ± 0.10	25.91 ± 0.16	24.97 ± 0.21	25.88 ± 0.14	24.49 ± 0.15	25.23 ± 0.08	24.44 ± 0.08
6	25.41 ± 0.14	24.42 ± 0.11	25.05 ± 0.08	24.40 ± 0.10	25.84 ± 0.15	24.73 ± 0.16	25.50 ± 0.11	24.70 ± 0.10
7	25.73 ± 0.13	...	24.87 ± 0.07	...	25.79 ± 0.19	...	25.83 ± 0.25	...
8	25.65 ± 0.13	...	25.34 ± 0.10	...	25.02 ± 0.08	...	25.10 ± 0.10	...
9	24.83 ± 0.07	...	25.74 ± 0.17	...	25.28 ± 0.08	...	25.31 ± 0.08	...
10	25.61 ± 0.13	24.44 ± 0.11	25.70 ± 0.16	25.46 ± 0.37	25.99 ± 0.19	24.72 ± 0.16	25.88 ± 0.13	24.70 ± 0.17
11	25.71 ± 0.14	...	25.01 ± 0.07	...	25.75 ± 0.25	...	24.90 ± 0.06	...
12	25.06 ± 0.08	24.27 ± 0.10	25.58 ± 0.12	25.05 ± 0.18	25.38 ± 0.09	24.39 ± 0.09	25.64 ± 0.16	24.93 ± 0.16
	36040		54700		55146		55599	
1	25.88 ± 0.16	24.71 ± 0.18	24.49 ± 0.05	23.43 ± 0.05	24.74 ± 0.11	23.85 ± 0.06	24.95 ± 0.06	24.00 ± 0.07
2	26.06 ± 0.20	25.08 ± 0.22	24.36 ± 0.11	23.53 ± 0.05	25.12 ± 0.11	24.28 ± 0.10	25.28 ± 0.08	24.34 ± 0.09
3	25.30 ± 0.09	...	23.89 ± 0.03	...	25.34 ± 0.09	...	25.50 ± 0.12	...
4	25.36 ± 0.09	...	23.83 ± 0.07	...	25.20 ± 0.08	...	25.73 ± 0.12	...
5	25.62 ± 0.11	24.57 ± 0.12	23.88 ± 0.04	23.09 ± 0.03	24.40 ± 0.04	23.61 ± 0.05	25.76 ± 0.16	24.50 ± 0.10
6	25.50 ± 0.24	24.51 ± 0.14	23.99 ± 0.03	23.08 ± 0.03	24.52 ± 0.05	23.67 ± 0.05	24.71 ± 0.05	23.86 ± 0.07
7	26.00 ± 0.17	...	24.05 ± 0.04	...	24.55 ± 0.05	...	24.67 ± 0.05	...
8	26.02 ± 0.16	...	24.07 ± 0.05	...	24.92 ± 0.06	...	24.93 ± 0.06	...
9	26.11 ± 0.25	...	24.23 ± 0.04	...	25.13 ± 0.07	...	25.08 ± 0.06	...
10	25.09 ± 0.07	24.09 ± 0.10	24.42 ± 0.05	23.32 ± 0.04	25.47 ± 0.12	23.75 ± 0.16	25.49 ± 0.09	24.41 ± 0.09
11	25.49 ± 0.10	...	24.38 ± 0.05	...	25.28 ± 0.15	...	25.67 ± 0.13	...
12	25.73 ± 0.12	24.62 ± 0.14	24.54 ± 0.10	23.49 ± 0.05	24.46 ± 0.04	23.62 ± 0.05	25.24 ± 0.07	24.04 ± 0.06
	55605		55614		55961		56190	
1	24.82 ± 0.07	24.06 ± 0.07	25.66 ± 0.14	24.60 ± 0.13	25.58 ± 0.11	24.45 ± 0.11	25.06 ± 0.07	24.42 ± 0.13
2	25.28 ± 0.12	24.19 ± 0.09	25.36 ± 0.08	24.31 ± 0.08	26.43 ± 0.26	24.46 ± 0.12	26.04 ± 0.17	24.56 ± 0.18
3	25.60 ± 0.11	...	25.88 ± 0.13	...	25.03 ± 0.27	...	25.27 ± 0.08	...
4	25.56 ± 0.13	...	24.63 ± 0.05	...	24.96 ± 0.07	...	25.76 ± 0.12	...
5	25.64 ± 0.11	24.20 ± 0.14	24.75 ± 0.05	23.90 ± 0.13	25.09 ± 0.08	23.91 ± 0.06	25.74 ± 0.11	24.63 ± 0.20
6	24.74 ± 0.05	23.97 ± 0.06	25.22 ± 0.09	24.20 ± 0.09	25.06 ± 0.07	23.94 ± 0.06	25.72 ± 0.11	24.51 ± 0.15
7	24.75 ± 0.06	...	25.66 ± 0.11	...	25.47 ± 0.12	...	25.06 ± 0.06	...
8	25.06 ± 0.07	...	25.72 ± 0.11	...	25.40 ± 0.11	...	25.52 ± 0.10	...
9	25.34 ± 0.11	...	24.69 ± 0.05	...	25.45 ± 0.09	...	25.79 ± 0.15	...
10	26.28 ± 0.32	24.59 ± 0.36	25.34 ± 0.08	24.09 ± 0.09	25.82 ± 0.14	24.25 ± 0.09	25.17 ± 0.09	24.18 ± 0.12
11	25.79 ± 0.14	...	25.56 ± 0.10	...	25.69 ± 0.13	...	25.42 ± 0.09	...
12	24.92 ± 0.07	24.08 ± 0.08	24.72 ± 0.05	23.94 ± 0.06	25.93 ± 0.14	24.67 ± 0.14	25.63 ± 0.10	24.57 ± 0.16
	56430		56762		56966		57127	
1	25.37 ± 0.11	24.55 ± 0.13	25.80 ± 0.12	24.79 ± 0.12	26.20 ± 0.25	25.03 ± 0.16	25.11 ± 0.10	24.55 ± 0.10
2	25.97 ± 0.18	24.62 ± 0.22	25.15 ± 0.07	24.36 ± 0.16	25.12 ± 0.10	24.48 ± 0.12	26.38 ± 0.21	25.08 ± 0.16
3	25.48 ± 0.09	...	26.02 ± 0.14	...	26.24 ± 0.25	...	25.97 ± 0.15	...
4	25.62 ± 0.10	...	26.02 ± 0.14	...	26.06 ± 0.16	...	26.01 ± 0.19	...
5	25.77 ± 0.12	24.71 ± 0.16	26.36 ± 0.18	24.86 ± 0.12	26.34 ± 0.19	25.20 ± 0.19	26.63 ± 0.24	25.03 ± 0.15
6	26.17 ± 0.45	24.70 ± 0.15	25.07 ± 0.07	24.30 ± 0.07	25.19 ± 0.09	...	26.09 ± 0.32	24.84 ± 0.12
7	25.81 ± 0.14	...	25.38 ± 0.12	...	24.92 ± 0.21	...	25.31 ± 0.30	...
8	24.84 ± 0.08	...	25.57 ± 0.10	...	25.53 ± 0.12	...	26.07 ± 0.19	...
9	25.51 ± 0.11	...	25.99 ± 0.13	...	25.73 ± 0.19	...	26.33 ± 0.18	...
10	26.09 ± 0.17	24.81 ± 0.15	25.97 ± 0.16	24.95 ± 0.16	26.06 ± 0.18	24.59 ± 0.12	25.52 ± 0.12	24.35 ± 0.08
11	25.27 ± 0.08	...	25.25 ± 0.07	...	25.14 ± 0.10	...	25.82 ± 0.14	...
12	25.38 ± 0.10	24.31 ± 0.13	25.86 ± 0.14	24.44 ± 0.12	25.61 ± 0.12	24.59 ± 0.16	25.20 ± 0.07	24.37 ± 0.11

Table 7—Continued

Epoch	<i>V</i>	<i>I</i>	<i>V</i>	<i>I</i>	<i>V</i>	<i>I</i>	<i>V</i>	<i>I</i>
	58373							
1	25.32 ± 0.11	24.52 ± 0.25						
2	26.96 ± 0.37	25.15 ± 0.17						
3	25.43 ± 0.17	...						
4	25.79 ± 0.11	...						
5	26.41 ± 0.19	25.23 ± 0.24						
6	26.39 ± 0.26	25.19 ± 0.17						
7	26.51 ± 0.26	...						
8	25.50 ± 0.10	...						
9	26.27 ± 0.17	...						
10	26.50 ± 0.25	25.46 ± 0.23						
11	25.58 ± 0.09	...						
12	26.58 ± 0.23	25.09 ± 0.38						

Table 8. Properties of Cepheid Variables in NGC 1637

ID	$P$ (days)	$\log P$	$\langle V \rangle$ (mag)	$\langle I \rangle$ (mag)	$A_V$ (mag)	$\mu_V$ (mag)	$\mu_I$ (mag)	$\mu_W$ (mag)
163 <sup>a</sup>	35.07	1.54	24.60	23.63	0.42	30.32	30.15	29.896
282 <sup>a</sup>	35.59	1.55	25.00	23.96	0.59	30.74	30.50	30.148
338 <sup>a</sup>	33.49	1.52	25.14	24.15	0.50	30.81	30.60	30.310
388 <sup>a</sup>	36.57	1.56	25.19	24.18	0.52	30.96	30.75	30.439
540 <sup>a</sup>	24.13	1.38	25.49	24.66	0.16	30.76	30.69	30.596
614	13.87	1.14	25.57	24.81	0.12	30.18	30.13	30.057
706	19.54	1.29	25.79	24.81	0.57	30.81	30.58	30.241
721	21.28	1.33	25.70	24.76	0.45	30.82	30.64	30.372
834	13.57	1.13	25.91	24.88	0.78	30.50	30.18	29.721
852	12.31	1.09	25.93	24.98	0.61	30.40	30.15	29.794
13638	19.38	1.29	25.28	24.42	0.29	30.29	30.17	30.003
13651 <sup>a</sup>	28.80	1.46	25.29	24.18	0.83	30.78	30.44	29.949
13923 <sup>a</sup>	32.84	1.52	25.37	24.40	0.45	31.01	30.83	30.565
13938	21.83	1.34	25.41	24.54	0.28	30.56	30.45	30.278
14003	15.26	1.18	25.34	24.43	0.47	30.06	29.87	29.597
14171 <sup>a</sup>	26.91	1.43	25.50	24.50	0.55	30.90	30.68	30.355
14256	15.80	1.20	25.62	24.87	0.06	30.39	30.36	30.325
14575	19.47	1.29	25.84	24.85	0.60	30.86	30.61	30.260
34707 <sup>a</sup>	50.29	1.70	24.38	23.41	0.36	30.53	30.39	30.178
34852 <sup>a</sup>	42.42	1.63	24.63	23.63	0.44	30.58	30.40	30.133
35053 <sup>a</sup>	31.46	1.50	24.92	23.76	0.91	30.51	30.14	29.602
35297	22.88	1.36	25.09	24.11	0.54	30.30	30.08	29.754
35576 <sup>a</sup>	23.15	1.36	25.22	24.20	0.63	30.44	30.18	29.809
35613	21.13	1.32	25.24	24.42	0.16	30.35	30.28	30.186
35713	17.05	1.23	25.39	24.53	0.30	30.24	30.12	29.943
35797	20.66	1.32	25.37	24.58	0.11	30.46	30.41	30.347
35834	19.35	1.29	25.47	24.55	0.45	30.48	30.30	30.033
35875	15.35	1.19	25.41	24.66	0.06	30.14	30.12	30.081
36040 <sup>a</sup>	31.71	1.50	25.59	24.52	0.68	31.19	30.91	30.506
54700 <sup>a</sup>	54.42	1.74	24.19	23.25	0.27	30.44	30.33	30.171
55146 <sup>a</sup>	32.66	1.51	24.91	23.97	0.38	30.55	30.39	30.173
55599 <sup>a</sup>	33.58	1.53	25.17	24.22	0.40	30.84	30.68	30.448
55605 <sup>a</sup>	32.57	1.51	25.22	24.23	0.49	30.85	30.65	30.364
55614	19.22	1.28	25.26	24.31	0.50	30.26	30.05	29.755
55961 <sup>a</sup>	48.85	1.69	25.43	24.15	1.12	31.55	31.09	30.433
56190	15.47	1.19	25.48	24.43	0.81	30.22	29.89	29.412
56430	20.00	1.30	25.48	24.48	0.60	30.53	30.28	29.923
56762	21.10	1.32	25.58	24.53	0.74	30.69	30.39	29.952
56966	22.41	1.35	25.58	24.62	0.50	30.76	30.56	30.267
57127	15.14	1.18	25.76	24.70	0.82	30.48	30.14	29.657
58373	16.90	1.23	25.99	24.96	0.73	30.83	30.54	30.104

<sup>a</sup>Used in final distance determination.

Table 9. NGC 1637 Distance Estimates

Technique	Distance (Mpc)	References
EPM	$7.86 \pm 0.50$ (statistical)	1, 2, 3
Cepheids	$11.71 \pm 0.99$	4
<i>B</i> -band TF	$13.8 \pm 2.4$	5
Inner ring	$11.12 \pm 3.53$	6
Kinematic	$10.7 \pm 2.4$ (statistical)	7
SEAM (preliminary)	$15.8 \pm 5.7$	8
SCM	$13 \pm 4$	9
Plateau-tail	$11.1 \pm 2.2$ (statistical)	10
BRSG	$7.8 \pm 2.1$	11

References. — (1) Hamuy et al. 2001; (2) Leonard et al. 2002a; (3) Elmhamdi et al. 2003; (4) this work; (5) Bottinelli et al. 1985; (6) Buta & de Vaucouleurs 1983; (7) Hamuy 2003; (8) E. Baron et al., in preparation; (9) Hamuy & Pinto 2002; (10) Nadyozhin 2003; (11) Sohn & Davidge 1998.

This figure "f5a.gif" is available in "gif" format from:

<http://arxiv.org/ps/astro-ph/0305259v1>

This figure "f5b.gif" is available in "gif" format from:

<http://arxiv.org/ps/astro-ph/0305259v1>

This figure "f5c.gif" is available in "gif" format from:

<http://arxiv.org/ps/astro-ph/0305259v1>

This figure "f5d.gif" is available in "gif" format from:

<http://arxiv.org/ps/astro-ph/0305259v1>

This figure "f5e.gif" is available in "gif" format from:

<http://arxiv.org/ps/astro-ph/0305259v1>

This figure "f5f.gif" is available in "gif" format from:

<http://arxiv.org/ps/astro-ph/0305259v1>

This figure "f5g.gif" is available in "gif" format from:

<http://arxiv.org/ps/astro-ph/0305259v1>

This figure "f5h.gif" is available in "gif" format from:

<http://arxiv.org/ps/astro-ph/0305259v1>

This figure "f5i.gif" is available in "gif" format from:

<http://arxiv.org/ps/astro-ph/0305259v1>